RICE UNIVERSITY

Improved Spectral Calculations for Discrete Schrödinger Operators

by

Charles Puelz

A Thesis Submitted
in Partial Fulfillment of the
Requirements for the Degree

Master of Arts

Approved, Thesis Committee:

Mark Embree, Chair
Professor of Computational and Applied Mathematics

Danny Sorensen
Noah Harding Professor of Computational and Applied Mathematics

---

David Damanik
Professor of Mathematics

Houston, Texas

May, 2013

Contents

Illustrations

ABSTRACT

Improved Spectral Calculations for Discrete Schrödinger Operators

by

Charles Puelz

This work details an $O(n^2)$ algorithm for computing the spectra of discrete Schrödinger operators with periodic potentials. Spectra of these objects enhance our understanding of fundamental aperiodic physical systems and contain rich theoretical structure of interest to the mathematical community. Previous work on the Harper model led to an $O(n^2)$ algorithm relying on properties not satisfied by other aperiodic operators. Physicists working with the Fibonacci Hamiltonian, a popular quasicrystal model, have instead used a problematic dynamical map approach or a sluggish $O(n^3)$ procedure for their calculations. The algorithm presented in this work, a blend of well-established eigenvalue/vector algorithms, provides researchers with a more robust computational tool of general utility. Application to the Fibonacci Hamiltonian in the sparsely studied intermediate coupling regime reveals structure in canonical coverings of the spectrum that will prove useful in motivating conjectures regarding band combinatorics and fractal dimensions.

Acknowledgments

I am truly blessed for family's support and guidance. My parents gave me the gift of life and unconditional love. My brother is my best friend and motivator.

I thank all the students in the CAAM department at Rice. In particular, I am grateful for David Medina's help in scripting and Jeff Hokanson's patience in allowing me to bother him with all sorts of questions. Also, thanks to Jeff and Russell Carden for comments in preparation for my defense.

David Damanik and Danny Sorensen provided helpful advice and corrections to my thesis draft. Dr. Sorensen's coaching in the thesis writing course shaped my presentation of the content.

Many discussions with Paul Munger greatly contributed to my understanding of this problem. I hope to continue our chats over coffee.

Lastly, I thank my advisor Mark Embree for introducing me to this neat eigenvalue problem and for his incredible mentoring ability.

Chapter 1

Background and Literature Review

Mathematical models of quantum systems present fascinating and subtle computational challenges. This thesis seeks to enable difficult spectral calculations of quantum mechanical operators by proposing an $O(n^2)$ computational tool of general utility and applying this tool to study a mathematical model of a quasicrystal, the Fibonacci Hamiltonian.

A typical finite difference approximation of the time-independent part of the Schrödinger equation, the canonical PDE in quantum mechanics, yields a special type of operator known variously as a Hamiltonian, tight-binding model, or discrete Schrödinger operator. Researchers in different fields study this object in several ways. Physicists interested in numerical simulations of quantum waves restrict the domain of this operator to a finite-dimensional subspace and evolve an initial state on a finite dimensional "lattice" with artificial absorbing boundary conditions. Mathematicians directly handle the infinite-dimensional operator with the goal of proving carefully formulated conjectures. Although different disciplines employ distinct approaches, researchers in both fields agree that spectra of these operators offer crucial insight into the modeled physical systems and contain rich structure interesting in its own right. First, working from the Schrödinger equation, I explain how one arrives at the

quantum model studied in this thesis.

1.1 Periodic Schrödinger operators

The Schrödinger Equation is

$$\imath\hbar\frac{\partial}{\partial t}\Psi(x,t) = (\Delta + V(x,t))\,\Psi(x,t).$$

Here $\hbar$ is Planck's constant, $V(x,t)$ is the potential, and $|\Psi(\cdot,t)|^2$ is the time dependent probability density of the quantum particle at time t. In the following, $\hbar$ is scaled to 1 and the potential is time-independent.

Let $\mathcal{H} = \Delta + V(x)$. A separation of variables approach with the assumption $\Psi(x,t) = \psi(x)\phi(t)$ results in a constant E and two equations, one in position, and one in time:

$$\mathcal{H}\psi = E\psi \tag{1.1}$$

$$\frac{\partial\phi}{\partial t} = \frac{-\imath E}{\hbar}\phi. \tag{1.2}$$

The first equation is known as the **Time Independent Schrödinger Equation** (TISE) and the operator $\mathcal{H}$ is called the Hamiltonian. To numerically approximate solutions to (1.1), it is natural to study another operator $\mathbf{H} : \ell^2(\mathbb{Z}) \to \ell^2(\mathbb{Z})$, a discretization of $\mathcal{H}$, defined as follows. Redefine $\psi \in \ell^2(\mathbb{Z})$ and take

$$(\mathbf{H}\psi)_n = \psi_{n-1} + v_n\psi_n + \psi_{n+1}. \tag{1.3}$$

The discrete approximation to the potential is $\{v_n\} \in \ell^\infty(\mathbb{Z})$, and a finite difference approximation to the Laplacian $\psi_{n+1} - 2\psi_n + \psi_{n-1}$ provides the off-diagonal terms in (1.3) (the scaling of the diagonal by 2 simply shifts the spectrum of $\mathbf{H}$ and is absorbed into the formula for v_n). This form of "approximation" to the Hamiltonian, called a *Jacobi operator*, serves as a fundamental quantum mechanical model and is the central focus of this work. A more general definition is given below:

Definition 1.1. *Let* $\{a_n\}$, $\{b_n\} \in \ell^\infty(\mathbb{Z})$. *A* ***Jacobi operator*** $\mathbf{J} : \ell^2(\mathbb{Z}) \to \ell^2(\mathbb{Z})$ *is defined as*

$$(\mathbf{J}\psi)_n = a_{n-1}\psi_{n-1} + b_n\psi_n + a_n\psi_{n+1}.$$

for all $\psi \in \ell^2(\mathbb{Z})$.

With the canonical basis $\{\mathbf{e}_n\}$ defined with 1 in the nth component and 0 otherwise, $\mathbf{J}$ can be displayed as the infinite dimensional tridiagonal matrix:

$$\mathbf{J} = \begin{bmatrix} \ddots & \ddots & \ddots & & & & \\ & a_{-2} & b_{-1} & a_{-1} & & & \\ & & a_{-1} & b_0 & a_0 & & \\ & & & a_0 & b_1 & a_1 & \\ & & & & \ddots & \ddots & \ddots \end{bmatrix}.$$

The sequences $\{a_n\}$ and $\{b_n\}$ are called the Jacobi *parameters*, and when $\{a_n\}$ is the constant sequence of 1's so $\mathbf{J}$ takes the form of equation (1.3), the operator is called a discrete one-dimensional *Schrödinger operator*.

A systematic study of the *spectrum* of particular Schrödinger operators provides significant physical insight into the corresponding quantum systems. The spectrum is defined as follows.

Definition 1.2. *The* ***spectrum*** *of* $\mathbf{J}$*, denoted* $\sigma(\mathbf{J})$ *is the following set of values:*

$$\sigma(\mathbf{J}) = \{\lambda : \mathbf{J} - \lambda\mathbf{I} \text{ does not have a bounded and densely defined inverse}\}.$$

The spectrum of $\mathbf{J}$ can be calculated from finite matrices if the Jacobi parameters satisfy a periodicity condition (see e.g. Teschl's book [25]). My algorithm described in Chapter 2 comes directly from this reformulation of the spectral calculation as a finite dimensional eigenvalue computation. More precisely, if for some $q \in \mathbb{Z}$, $a_n = a_{n+q}$ and similar for b_n, the spectrum is a union of q intervals whose endpoints are the eigenvalues of two matrices:

$$\mathbf{J}_{\pm} = \begin{bmatrix} b_1 & a_1 & & & \pm a_0 \\ a_1 & b_2 & \ddots & & \\ & \ddots & \ddots & \ddots & \\ & & \ddots & b_{q-1} & a_{q-1} \\ \pm a_0 & & & a_{q-1} & b_q \end{bmatrix}.$$

This fact is presented in the following Theorem.

Theorem 1.1. *Let* $\mathbf{J}$ *be a Jacobi operator with parameters* $\{a_n\}$ *and* $\{b_n\}$*. If these*

sequences are q-periodic, then

$$\sigma(\mathbf{J}) = \bigcup_{k=1}^{q} [E_{2k-1}, E_{2k}]$$

where the $E_1 < E_2 \leq E_3 < E_4 \leq \ldots \leq E_{2q-1} < E_{2q}$ *comprise* $\sigma(\mathbf{J}_+) \cup \sigma(\mathbf{J}_-)$.

The quasicrystal model investigated in Chapter 3, formulated as a Jacobi operator, contains aperiodic structure lying qualitatively in the middle of the extremes periodic and random. In turn, it is relevant to first understand a fundamental distinction between random and periodic quantum systems.

1.2 Random and Periodic Quantum Models

The potential sequence $\{v_n\}$ in (1.3) encodes properties of the quantum system to be modeled: researchers have thoroughly investigated the fundamental cases of periodic and random potentials. An example of the former potential would be v_n as the sequence $1, 0, 1, 0, 1, 0 \ldots$ and the latter would be constructing v_n as a uniform random number between 0 and 1 for each n. A periodic potential may be interpreted physically as a perfect crystal or pristine physical system, while a random potential is often meant to simulate a system with *impurities*, or imperfections. Understanding transport through random potentials is significant from a modeling perspective since experimental apparati are often far from ideal systems, containing "random" impurities in their construction. In turn, theoretical models designed to simulate these

experiments must take into account these impurities, and a good understanding of their effects in quantum systems is of crucial importance. Not surprisingly, periodic and random models exhibit different electronic transport properties.

The underlying distinction between these two types of models is the following: electrons transport well in periodic systems and poorly in random systems. Transport in periodic systems is called *ballistic* in certain contexts, and lack of diffusion in random systems is termed *Anderson localization* after the scientist Phillip Anderson, who wrote the seminal paper in this area [1]. The latter term refers to a literal localization in space of an electron wave spreading through the lattice.

Figure 1.1 displays an initial delta function evolved in time on both a periodic and random lattice. This simulation was performed in MATLAB by truncating the Hamiltonian to an order 1001 tridiagonal matrix, and evolving the initial state in time with the matrix exponential as given below:

$$\Psi(x,t) = \exp\left(-\frac{\imath}{\hbar}\mathbf{H}t\right)\Psi(x,0).$$

If the snapshots of the wavefunction on the random lattice are plotted on a log-linear scale, one would observe an exponential envelope encasing the wavefunction. This phenomenon is termed exponential localization, meaning that the tails of the wavefunction decay in a roughly exponential fashion. The snapshots on each row correspond to the same time and were chosen to demonstrate diffusion in the periodic case and as Anderson described it, the "absence of diffusion" in the random case [1].

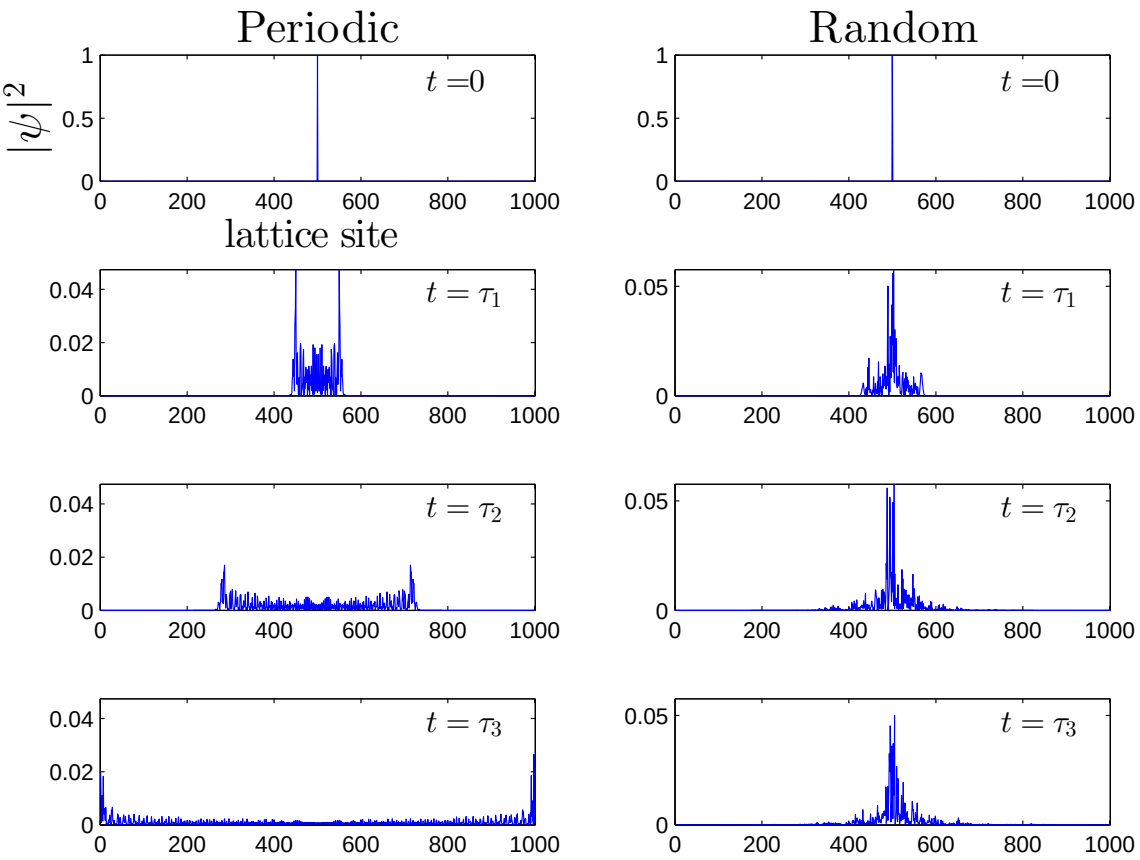

Figure 1.1 : Three snapshots in time of an evolving wave. Diffusion occurs in the periodic lattice and localization occurs in the random lattice.

1.3 Quasiperiodic Quantum Models

Several relevant quantum mechanical models have potentials that are determinstic, but not periodic, and so they fall in between the two extremes of periodic and random: these are called *quasiperiodic* or *aperiodic* models. It is natural to wonder how electrons move in these aperiodic structures: do they localize like in the random case,

diffuse as in the periodic case, or something in between? Answers to this question are often elusive and model dependent. Gaining insight into electronic properties of quasiperiodic systems is the motivation for my computational work discussed in Chapter 2.

Two of the more popular quasiperiodic Schrödinger operator models are the *Almost Mathieu* operator and the *Fibonacci Hamiltonian*. The Almost Mathieu operator, also called the *Harper model* in the physics literature, has a potential defined

$$v_n = \lambda \cos(2\pi\sigma n + \theta),$$

with $\lambda > 0$ and σ irrational. This potential $\{v_n\}$ is not periodic, and hence provides an example of a sequence in between the periodic and random. In the words of the luminous physicist D.J. Thouless, this model "describe[s] the quantum theory of an electron confined to a plane with a periodic potential in the plane and a uniform magnetic field perpendicular to the plane" [26]. Although not a focus, I mention this model since it has been the center of extensive research, some of which sets a precedent for my computational work. I will detail this information in the coming sections.

This work focuses on the Fibonacci Hamiltonian, perhaps one of the more popular *quasicrystal* models. Quasicrystals are peculiar objects that have attracted recent interest in part from their unique structure: deterministic but lacking translational symmetry. A Penrose tiling of $\mathbb{R}^2$ depicted in Figure 1.2 provides a famous example

of such a pattern.

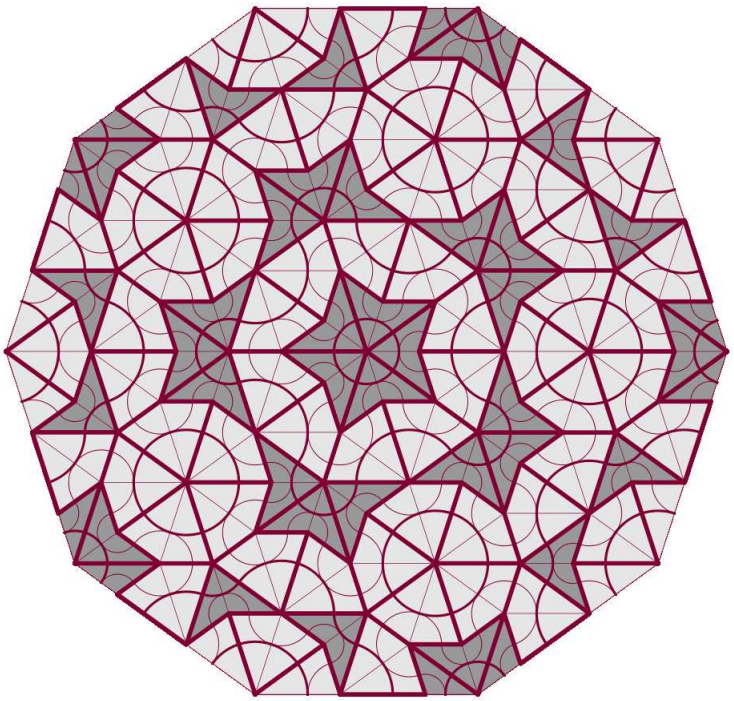

Figure 1.2 : Penrose tiling of the plane. URLs: `http://en.wikipedia.org/wiki/File:Penrose_sun_3.svg` and `http://en.wikipedia.org/wiki/Penrose_tiling`

Nadia Drake has written a nice historical overview of quasicrystals [9]. Synthetic quasicrystals appeared in labs in the 1980s, most notably in the Nobel prize winning work of Dan Shechtman [9]. Also during this time, Sütő and others led foundational theoretical research on models of quasicrystals, in particular the Fibonacci Hamiltonian [21, 22]. While experimentalists like Shechtman could produce these objects in labs, a lingering question remained: do quasicrystals exist in nature [9]? This question was answered only very recently with a paper published in 2009 by Steinhardt et al.:

these scientists reported their discovery of a rock originally located in Russia containing quasicrystals, and concluded it most likely came from an extraterrestrial source [9]. This recent discovery, along with foundational experimental and theoretical work begun in the 1980s, has pushed quasicrystals and their corresponding mathematical models to the forefront of research in mathematical physics.

The Fibonacci Hamiltonian is an example of a quasiperiodic model meant to capture the deterministic and nonperiodic structure of quasicrystals. With $\lambda > 0$ and $\phi = \frac{1}{2}(1 + \sqrt{5})$, the potential is

$$v_n = \lambda \chi_{[1-\phi^{-1},1)}(n\phi^{-1} \bmod 1).$$

Following the notation in the literature, let Σ_λ be the spectrum of the Fibonacci Hamiltonian. As rigorously shown by Sütő, the spectrum Σ_λ is a *Cantor set* of measure zero for all $\lambda > 0$ [22]. For completeness, I include the following definition (see Willard's book [30, p. 217]).

Definition 1.3. *A* ***Cantor set*** $\Sigma \subset \mathbb{R}$ *is perfect, compact, and totally-disconnected.*

Sütő proved several useful facts linking the spectrum of this model to spectra of closely related periodic Schrödinger operators. More precisely, let $\{F_k\}$ be a Fibonacci sequence of numbers ($F_k = F_{k-1} + F_{k-2}$) with $F_0 = 1$ and $F_1 = 1$, and consider another Schrödinger operator with potential

$$v_n^{(k)} = \lambda \chi_{[1-F_{k-1}/F_k,1)}(nF_{k-1}/F_k \bmod 1).$$

In this case, one obtains the periodic Schrödinger operator by replacing the irrational number ϕ in the formula for v_n with a rational approximation F_k/F_{k-1}. As explained in the following theorem, this particular choice of a rational approximant yields periodic operators whose spectra, denoted σ_k, relate to the original Cantor spectrum Σ_λ in a well-understood way.

Theorem 1.2. *(Sütő, 1987, 1989.) For all $\lambda > 0$, Σ_λ is a measure zero Cantor set and the sets σ_k satisfy*

$$\sigma_k \cup \sigma_{k+1} \subset \sigma_{k-1} \cup \sigma_k \tag{1.4}$$

$$\Sigma_k = \bigcap_{k \geq 1} \sigma_k \cup \sigma_{k+1}. \tag{1.5}$$

It is known that Σ_λ is a *dynamically defined* Cantor set for λ large enough and small enough; see Definition 5.2 and Corollary 5.6 in the survey paper by Damanik, Embree, and Gorodetski for a summary of results [6]. Further, the authors conjecture that for all $\lambda > 0$, Σ_λ is dynamically defined. The precise definition given in the survey follows below [6]. Let $B \subset \mathbb{R}$ be a closed interval.

Definition 1.4. *(From the survey [6]) A **dynamically defined** Cantor set $\Sigma \subset B$ satisfies the following:*

there exist strictly monotone contracting maps $\psi_1, \psi_2, \ldots, \psi_j : B \to B$ so that

$$\psi_k(B) \cap \psi_l(B) = \emptyset \text{ provided } k \neq l,$$

and with $B_1 = \psi_1(B) \cup \cdots \psi_j(B)$, $B_{n+1} = \psi_1(B_n) \cup \cdots \cup \psi_j(B_n)$ *one has*

$$\Sigma = \bigcap_{n \geq 1} B_n.$$

A simple example of such a Cantor set is the famous "middle thirds" Cantor set, obtained by iteratively removing the middle third from a sequence of intervals, and then intersecting the remaining sets. In this case, $B = [0, 1]$ and the contracting maps used in the construction are $\psi_1(x) = \frac{1}{3}x$ and $\psi_2(x) = \frac{1}{3}x + \frac{2}{3}$

The Cantor structure of the spectrum as formulated in Theorem 1.2 is a profound result and perhaps surprising at first glance. Peering at this operator instead through the lense of dynamical systems enhances one's intuition: values in the spectrum Σ_λ (and covers $\sigma_k \cup \sigma_{k+1}$) relate to bounded sequences of a particular map. This fact was also shown by Sütő [21].

Theorem 1.3. *Fix* $\lambda > 0$ *and* $E \in \mathbb{R}$. *Let* $\{x_k\}$ *be a sequence of numbers with the initial conditions* $x_{-1} = 2$, $x_0 = E$, $x_1 = E - \lambda$, *and satisfying* $x_{k+1} = x_k x_{k-1} - x_{k-2}$. *Then:*

$$\sigma_k = \{E : |x_k(E)| \leq 2\} \text{ and}$$

$$\Sigma_\lambda = \{E : \sup_k |x_k(E)| < \infty\}.$$

Although the algorithm I present in Chapter 2 is general, the motivation for my computational work applied to the Fibonacci Hamiltonian relies on the theoretical foundation provided by Theorem 1.2 and 1.3. More precisely, to enable numerical

calculations, one takes the covers $\sigma_k \cup \sigma_{k+1}$ as approximations to the original Cantor spectrum Σ_λ, and then from these covers extracts approximations of interesting quantities. These "interesting quantities", like fractal dimensions, provide physical insight into quasicrystals and thus encourage a careful study of the spectrum Σ_λ.

1.4 Why study the spectrum?

Physicists and mathematicians glean useful theoretical and physical intuition by studying the spectrum of quantum models. Work from physicists has related fractal dimensions of spectra to time dependent quantities associated with the wave function $\Psi(x,t)$ (see e.g. [20, 15, 14, 29]). Numerical results suggest a connection between temporal behavior and fractal dimensions of spectra *and* of the wave functions, although I note that some researchers have provided numerical evidence weakening the former connnection in certain contexts [29]. Regardless, spectral computations are useful in studying "crictical level statisitics" of relevant quantum models [23, 5, 19].

More recently, mathematicians have developed rigorous results for time-dependent behavior: see the work of Damanik et al. for a result incoporating the fractal dimension of the spectrum [7]. In addition, theoreticians enjoy and work to rigorously explain the mathematical beauty inherent in models and their spectra; the Fibonacci Hamiltonian is a prime example of such a model containing rich theoretical structure, as touched upon in Theorems 1.2 and 1.3. Thus, future work on such models and their spectra will refine our understanding of the electronic properties of quasicrystals and

other aperiodic systems, lead to real world applications, and reveal interesting mathematics. My computational work will aide in these endeavors. First, I will discuss previous computational work on quasiperiodic Schrödinger operator models.

1.5 Previous computational work on aperiodic models

In this section I detail the computational work done for approximating the spectrum of versions of the Harper model and Fibonacci Hamiltonian. The general theme for numerical calculations is to take a rational approximant to the irrational parameter appearing in the formula for the potential, and then compute the spectrum of the corresponding periodic Schrödinger operator. One hopes that the spectrum of the periodic operator accurately approximates the original spectrum. More specifically, in the Fibonacci Hamilonian, ϕ is approximated by F_k/F_{k-1}, and in the Harper model, σ is approximated by a close rational p/q, in both cases resulting in a periodic potential. For the Fibonacci and Harper models, Theorem 1.2 provides a way to tackle the spectral calculation of the periodic operator with an eigenvalue algorithm applied to $\mathbf{J}_{\pm}$. In the Fibonacci case, Theorem 1.3 provides an additional method to compute the spectrum via a root-finding algorithm for $x_k(E) - 2$ and $x_k(E) + 2$ [6].

Obtaining a "good approximation" to the Cantor spectrum (for example, in the sense of equations (1.4) and (1.5) for the Fibonacci Hamiltonian) requires large k, or equivalently considering periodic approximations to the potential of increasingly long period. Figures 1.4 and 1.3 demonstrate the convergence of the covers $\sigma_k \cup \sigma_{k+1}$

to the Cantor spectrum for the Fibonacci model by displaying exponential decay of interval widths and minimum gap widths. Here, $k = 25$, so the largest eigenproblem to be solved is of size $F_{26} = 196418$. Thus, computation of well-approximating periodic spectra via calculation of the eigenvalues of $\mathbf{J}_{\pm}$ becomes an extremely large eigenvalue problem. Further, for λ sufficiently small, one can can consider even larger problems due to the slower decay of band sizes in the covers $\sigma_k \cup \sigma_{k+1}$. Such largescale computations are not scalable via common algorithms requiring $O(n^3)$ floating point operations (flops). For example, an application of the QR algorithm first requires $O(n^3)$ flops to reduce $\mathbf{J}_{\pm}$ to similar tridiagonal matrices and then $O(n^2)$ flops to compute the eigenvalues.

In light of the challenge of largescale eigenvalue computations, physicists performing calculations for Fibonacci-type models have often resorted to a study of latter method: the dynamical map (e.g. [19, 17, 15]). As explained in the paper by Damanik et al., computations in this context present their own challenges [6]. The authors note that in the Fibonacci Hamiltonian model, the polynomial in E, $x_k(E)$, has coefficients quickly tending to infinity as k tends to infinity. Further, the slope of $x_k(E)$ becomes arbitrarily large in the regions where it is bounded in magnitude by 2, since the intervals in the spectrum of the periodic approximations converge to a Cantor set. These properties destroy the utility of root-finding calculations.

Researchers have directly tackled the large scale eigenvalue problem for the Harper model by constructing a similarity transformation converting $\mathbf{J}_{\pm}$ to tridiagonal form;

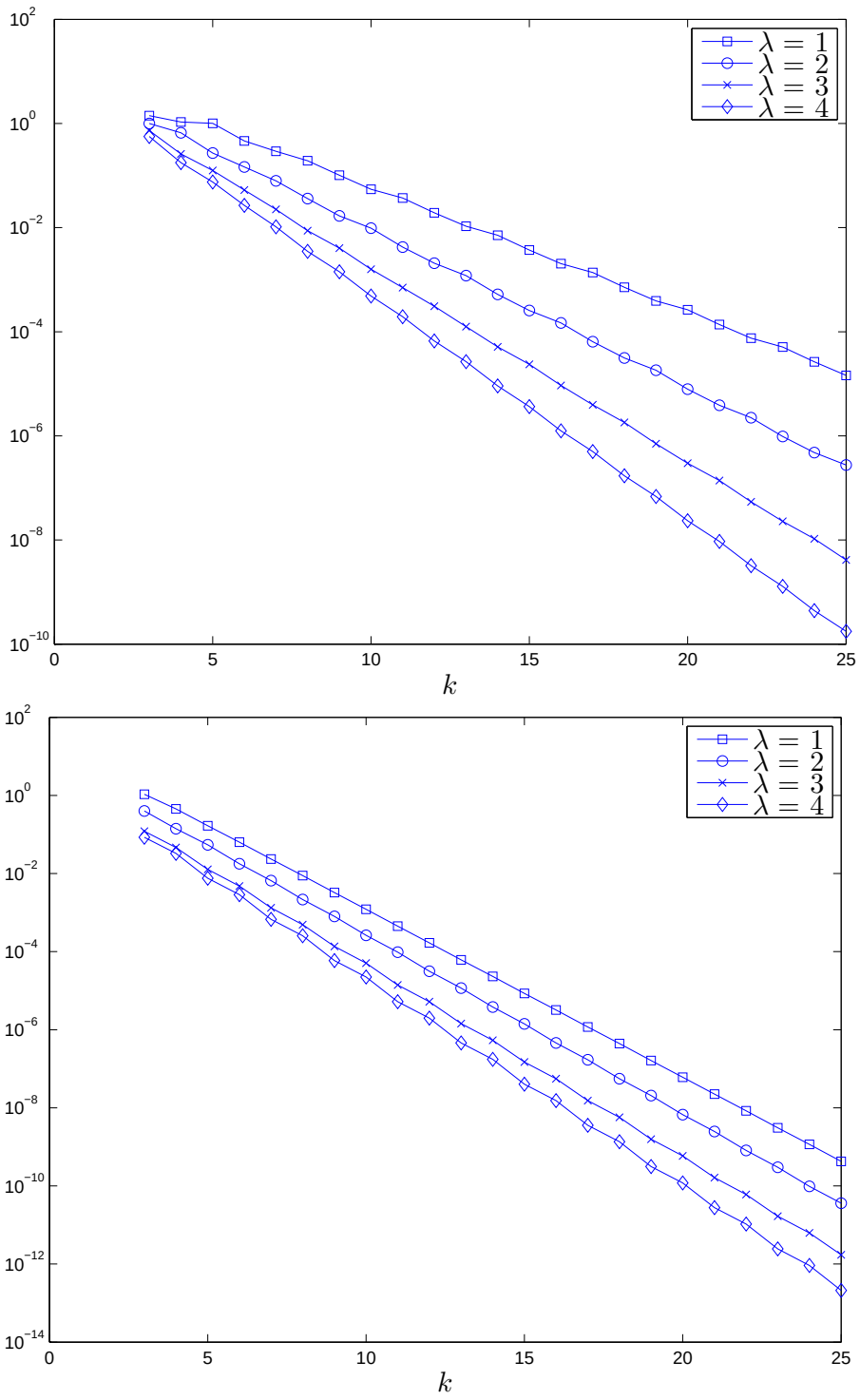

Figure 1.3 : Maximum interval length (top) and minimum interval length (bottom) in $\sigma_k \cup \sigma_{k+1}$.

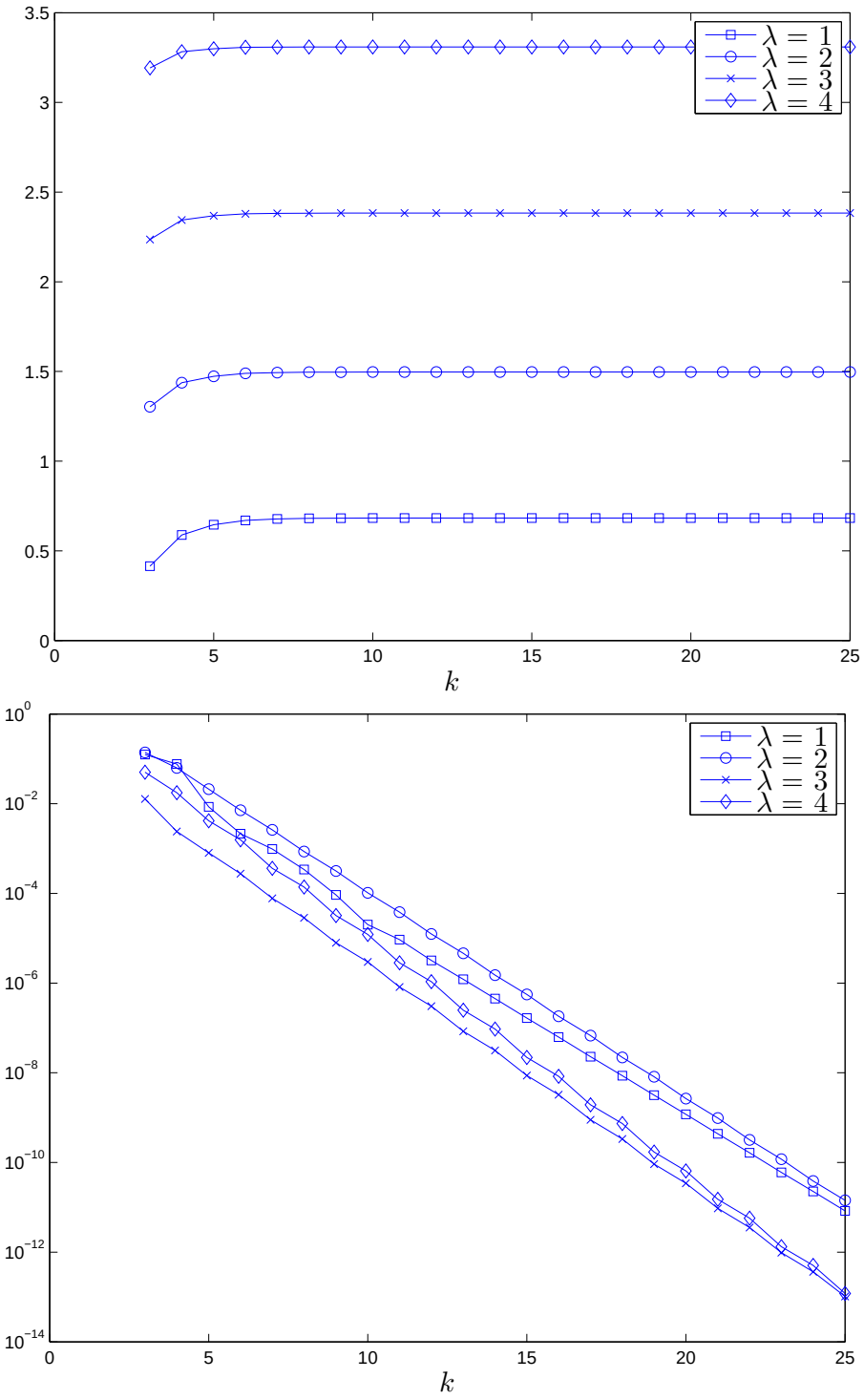

Figure 1.4 : Maximum gap length (top) and minimum gap length (bottom) in $\sigma_k \cup \sigma_{k+1}$.

an application of the QR algorithm computes the eigenvalues of this tridiagonal reduction in $O(n^2)$ flops. Partial work toward this end can be seen in the early paper of Thouless [26]. In 1997, Lamoureux published a paper detailing a complete construction of the similarity transformation for a more general class of matrices, and the Harper model fits this mold [18]. Takada et al. presented a solution in 2004, as applied to a different but closely related version of the Harper model, apparently unaware of Lamoureux's work [23]. The work of Lamoureux and Takada et al. rely on special properties of the potential that do not hold for the Fibonacci Hamiltonian.

Since calculation with the dynamical map can be problematic, recent numerical work for the Fibonacci Hamiltonian uses an eigenvalue algorithm applied directly to $\mathbf{J}_{\pm}$; these computations appear for example in the research of Mandel and Lifshitz and Damanik, Embree, and Gorodetski [6, 10, 11]. My work provides these researchers and others with a tool to push these numerical computations to higher, more accurate levels (in the sense of approximating the spectrum of the quasiperiodic operator). The algorithm detailed below computes the spectrum of $\mathbf{J}_{\pm}$ in $O(n^2)$ flops with $O(n)$ storage and requires no assumptions on the Jacobi parameters. It can be applied to any periodic Schrödinger operator whose spectrum approximates an aperiodic model. To the best of my knowledge, this is the first available $O(n^2)$ algorithm available for calculation of the covers $\sigma_k \cup \sigma_{k+1}$ for the spectrum of the Fibonacci Hamiltonian.

Chapter 2

Algorithm for Computing Schrödinger Spectra

Following from the previous section, to approximate the Cantor spectrum Σ_λ by the canonical covers $\sigma_k \cup \sigma_{k+1}$, I wish to compute all the eigenvalues of matrices of the following structure:

$$\mathbf{J}_\pm = \begin{bmatrix} b_1 & a_1 & & & \pm a_0 \\ a_1 & b_2 & \ddots & & \\ & \ddots & \ddots & \ddots & \\ & & \ddots & b_{q-1} & a_{q-1} \\ \pm a_0 & & & a_{q-1} & b_q \end{bmatrix}. \tag{2.1}$$

The proposed algorithm is formulated with these matrices $\mathbf{J}_\pm$. Recall that the $2q$ sorted eigenvalues of (2.1) give the endpoints of the intervals comprising the spectrum of the q-periodic Jacobi operator with parameters $\{a_n\}$ and $\{b_n\}$. The corners entries $\pm a_0$ complicate reduction of $\mathbf{J}_\pm$ to tridiagonal form via orthogonal transformations. For example, a naive implementation of Givens rotations to "push" the corner entries inward fills in the upper and lower portions of the matrix with nonzero values. As noted, working from the structure of the almost Mathieu model, Lamoureux and Takada et al. were able to elegantly avoid this difficulty by building orthogonal

matrices transforming $\mathbf{J}_\pm$ to tridiagonal form [18, 23]. These approaches utilize certain properties of the almost-Mathieu potential and are not immediately generalizable to other operators like the Fibonacci Hamiltonian.

Instead of utilizing an explicitly constructed orthogonal transformation, my algorithm splits $\mathbf{J}_\pm$ into a tridiagonal plus low-rank modification. This technique maintains generality: it can be used to compute the spectrum of any periodic Jacobi operator, and has a similar flavor to previous work in eigenvalue computations [4, 2, 12, 3].

I will begin with a detailed discussion of the algorithm, called Algorithm 1, followed by some timing results. This chapter concludes with two tests of the algorithm. The first test applies Algorithm 1 to special matrices for which I have an closed form for their eigenvalues, and the second to the Fibonacci Hamiltonian model to compute $\sigma_k \cup \sigma_{k+1}$.

2.1 Algorithm

This algorithm is presented for the matrix $\mathbf{J}_+$; the one for $\mathbf{J}_-$ is equivalent. First, consider the splitting:

$$\mathbf{J}_+ = \underbrace{\begin{bmatrix} b_1 - a_0 & a_1 & & & & \\ a_1 & b_2 & \ddots & & & \\ & \ddots & \ddots & \ddots & & \\ & & \ddots & b_{q-1} & a_{q-1} & \\ & & & a_{q-1} & b_q - a_0 \end{bmatrix}}_{\mathbf{T}} + \mathbf{w}\mathbf{w}^*$$

with $\mathbf{w} = \sqrt{a_0}(\mathbf{e}_1 + \mathbf{e}_n)$.

Let the diagonalization of $\mathbf{T}$ be denoted $\mathbf{Q}\mathbf{D}\mathbf{Q}^*$. Then $\mathbf{J}_+$ is similar to $\mathbf{D} + \mathbf{z}\mathbf{z}^*$, where $\mathbf{z} = \mathbf{Q}^*\mathbf{w}$. With this notation, the algorithm takes the following form:

Algorithm 1: Computing spectrum of a periodic Jacobi operator

1. Compute all eigenvalues of $\mathbf{T}$ with the QR algorithm (`DSTERF.f`).

2. Sequentially compute the eigenvectors of $\mathbf{T}$ via inverse iteration, and store the first and last components. The vector $\mathbf{z}$ is calculated from these stored components (`DSTEIN.f`).

3. For the eigenvalues of $\mathbf{D}$ such that the corresponding component of $\mathbf{z}$ is nonzero, solve the secular equation associated with $\mathbf{D} + \mathbf{z}\mathbf{z}^*$ with a Newton-type method (`DLAED4.f` plus code to account for deflation).

2.2 Explanation of subparts

It can be shown that each step in Algorithm 1 takes $O(n^2)$ flops. Below, I detail some important facts and references for each subpart: QR iteration, inverse iteration, and root-finding for the secular equation. For details regarding this standard material in numerical linear algebra, see[27, pp. 202-233] and [8]. Included in description of Algorithm 1 are the LAPACK routines used in my implementation.

2.2.1 QR algorithm

The QR iteration for eigenvalue computations is an iterative method based on taking the QR factorization of a matrix. At its simplest, the iteration takes the following form:

QR iteration

1. Reduce $\mathbf{A}$ to upper Hessenberg form $\mathbf{B}$ (tridiagonal if $\mathbf{A}$ is Hermitian).
2. Let $\mathbf{B}^{(0)} := \mathbf{B}$. Iterate until $\mathbf{B}^{(n)}$ converges to an upper triangular matrix (diagonal if $\mathbf{A}$ is Hermitian):
   (a) QR factorization: $\mathbf{Q}^{(n)}\mathbf{R}^{(n)} = \mathbf{B}^{(n-1)}$.
   (b) $\mathbf{B}^{(n)} := \mathbf{R}^{(n)}\mathbf{Q}^{(n)}$. Go to (a).

Several important modifications vastly improve convergence. Implementations of this algorithm factor a shifted matrix at step 2(a), and with minor additions,

convergence is achieved in $O(n^2)$ operations. Further if λ_l and $\tilde{\lambda}_l$ are the exact and computed eigenvalues, and $\varepsilon_{\text{mach}}$ is machine epsilon, then

$$\frac{|\lambda_l - \tilde{\lambda}_l|}{\|A\|} = O(\varepsilon_{\text{mach}}).$$

I use LAPACK's `DSTERF.f`, a eigenvalue routine for symmetric tridiagonal matrices, in my implementation of Algorithm 1.

2.2.2 Inverse iteration

The inverse iteration procedure for computing eigenvector components corresponding to an eigenvalue γ in second step of Algorithm 1 is simply the power method applied to the matrix $(\mathbf{A} - \alpha\mathbf{I})^{-1}$. Here $\alpha \approx \gamma$, implying the eigenvalue of largest magnitude is $1/(\gamma - \alpha)$ and the power method converges to the corresponding eigenvector.

Inverse iteration

Let $\mathbf{x}^{(0)}$ be an initial normalized vector. Iterate until convergence:

1. Solve $(\mathbf{A} - \alpha\mathbf{I})\mathbf{y}^{(n)} = \mathbf{x}^{(n-1)}$ for $\mathbf{y}^{(n)}$.

2. $\mathbf{x}^{(n)} = \mathbf{y}^{(n)}/\|\mathbf{y}^{(n)}\|$. Go to 1.

Now assume $\mathbf{A}$ is tridiagonal. In this case, steps 1 and 2 cost $O(n)$ flops. With α chosen as the computed eigenvalue from step 1, the convergence to the corresponding eigenvector is extremely fast, given suitable spacing between the eigenvalues [8, pp.

212, 231]. In turn, the cost for inverse iteration to compute all eigenvectors is $O(n^2)$ flops.

The caveat is the condition of "suitable separation" of the eigenvalues; nearby eigenvalues can yield inaccurately calculated eigenvectors. Further, as depicted in Figures 1.3 and 1.4, the Fibonacci model naturally yields close eigenvalues, since they approximate a set of measure zero. I remark here that I have not experienced difficulties with inverse iteration in the sense of numerical problems in step 2 polluting the final computed eigenvalues, but the proximity of the eigenvalues in my application means we should be vigilant for such problems. Demmel notes that research has indicated the possibility, "that inverse iteration may be 'repaired' to provide accurate, orthogonal eigenvectors without spending more than $O(n)$ flops per eigenvector " [8, p. 231]. In turn, future work may result in an improvement of Algorithm 1, step 2, with a more robust but equally efficient algorithm for eigenvectors.

My implementation of Algorithm 1 uses LAPACK's `DSTEIN.f`, a routine specilized for eigenvector calculations via inverse iteration for tridiagonal matrices.

2.2.3 Secular equation and timing results

Step 3 of Algorithm 1 requires computation of the eigenvalues of a diagonal matrix plus a symmetric rank-one modification. That is, compute δ so that

$$\det(\mathbf{D} + \mathbf{z}\mathbf{z}^* - \delta\mathbf{I}) = 0. \tag{2.2}$$

Several facts allows one to rewrite (2.2) in an equivalent form called the *secular equation*. Note that in this context, the eigenvalues of the matrices $\mathbf{D}$ and $\mathbf{D} + \mathbf{z}\mathbf{z}^*$ are real, since the former is similar to a Hermitian matrix and the latter itself is Hermitian.

Lemma 2.1. $\det(\mathbf{I} + \mathbf{x}\mathbf{y}^*) = 1 + \mathbf{y}^*\mathbf{x}$.

Proof. Begin with the following matrix equation:

$$\begin{bmatrix} \mathbf{I} & 0 \\ \mathbf{y}^* & 1 \end{bmatrix} \begin{bmatrix} \mathbf{I} & -\mathbf{x} \\ 0 & 1 + \mathbf{y}^*\mathbf{x} \end{bmatrix} = \begin{bmatrix} \mathbf{I} & -\mathbf{x} \\ 0 & 1 \end{bmatrix} \begin{bmatrix} \mathbf{I} + \mathbf{x}\mathbf{y}^* & 0 \\ \mathbf{y}^* & 1 \end{bmatrix}.$$

Taking the determinant of both sides and using the following properties:

- $\det(\mathbf{A}\mathbf{B}) = \det(\mathbf{A}) \det(\mathbf{B})$.
- $\det(\mathbf{A}) =$ product of the eigenvalues of $\mathbf{A}$.

results in the equation

$$1 + \mathbf{y}^*\mathbf{x} = \det \begin{bmatrix} \mathbf{I} + \mathbf{x}\mathbf{y}^* & 0 \\ \mathbf{y}^* & 1 \end{bmatrix} = \det(\mathbf{I} + \mathbf{x}\mathbf{y}^*) \blacksquare.$$

Lemma 2.2. *Let $d_1 < d_2 < \cdots < d_n$ and $\delta_1 \leq \delta_2 \leq \cdots \leq \delta_n$ be the eigenvalues of $\mathbf{D}$ and $\mathbf{D} + \mathbf{z}\mathbf{z}^*$ respectively, where $\mathbf{D}$ is diagonal. Then, if every component of $\mathbf{z}$ is nonzero, we have $d_1 < \delta_1 < d_2 < \delta_2 < \cdots < d_n < \delta_n$.*

Please refer to Wilkinson's *The Algebraic Eigenvalue Problem* for a discussion of the latter lemma [28, pp. 94-98]. From this point, without loss of generality I assume

that all the entries of $\mathbf{z}$ are nonzero. (If the jth component is equal to zero, then $d_j \in \sigma(\mathbf{D}+\mathbf{z}\mathbf{z}^*)$ with eigenvector $\mathbf{e}_j$, and the remaining problem can be split into two independent smaller problems. This reduction in dimension of the eigenproblem is sometimes called *deflation*. Let $\delta \in \sigma(\mathbf{D}+\mathbf{z}\mathbf{z}^*)$. By Lemma 2.2, $\mathbf{D}-\delta\mathbf{I}$ is invertible and one can write

$$\mathbf{D}+\mathbf{z}\mathbf{z}^*-\delta\mathbf{I} = (\mathbf{D}-\delta\mathbf{I})(\mathbf{I}+(\mathbf{D}-\delta\mathbf{I})^{-1}\mathbf{z}\mathbf{z}^*).$$

In turn, by Lemma 2.1, equation (2.2) is satisfied if and only if

$$g(\delta) := 1+\sum_{j=1}^{n}\frac{|z_j|^2}{d_j-\delta} = 0. \tag{2.3}$$

Equation (2.3) is called the *secular equation*. In this light, the eigenvalues of $\mathbf{D}+\mathbf{z}\mathbf{z}^*$ can be calculated by a root-finding algorithm applied to this equation. Work towards developing a sufficiently fast root-finder arose from the rank one modification to the symmetric eigenproblem, and later from the need to find zeros of (2.3) as a substep of the divide-and-conquer eigenvalue algorithm. Thus, Bunch, Nielsen, and Sorensen built an efficient Newton-type iteration by creating a rational function approximant to $g(\delta)$ [4] (summarized in [8, pp. 221-223] and [27, 229-232]). The LAPACK routine `DLAED4.f` encodes this particular root-finding algorithm and is what I use in my implementation of Algorithm 1.

I supplemented this routine with code to handle the case when a component of $\mathbf{z}$

is zero and the problem deflates. More precisely, if a component $|z_i| \leq \varepsilon_{\text{mach}}$, the code bypasses the root-finding procedure and the corresponding eigenvalue of $\mathbf{D} + \mathbf{z}\mathbf{z}^*$ is taken to be the unperturbed diagonal entry d_i of $\mathbf{D}$.

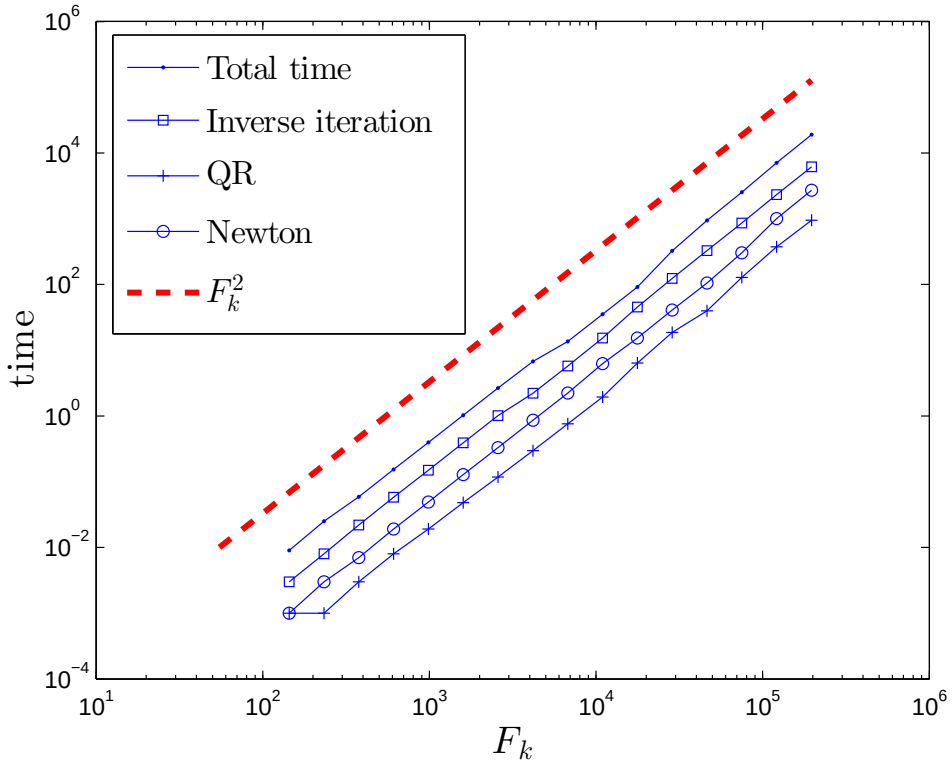

Figure 2.1 : Timing results for Alg. 1 applied to the Fibonacci model with double precision arithmetic. Displayed are the timing results for individual tests along with the total time.

Timing results for Algorithm 1 applied to compute σ_k for the Fibonacci Hamiltonian are displayed in Figure 2.1. Interestingly, step 2 and 3 both take greater time than the QR iteration for $\mathbf{T}$. This observation justifies the parallelization of step 2 and 3 for greater efficiency.

2.3 Testing and some comparisons

2.3.1 Gear matrices

In 1969 paper, C.W. Gear carefully calculates closed-form expressions for the eigenvalues of matrices that are tridiagonal plus small modifications to their first and last rows. Such examples include the matrices $\mathbf{J}_{\pm}$ with the Jacobi parameters $a_n = 0$ and $b_n = 1$. Using his notation, let an even number N be the order of the matrix. The eigenvalues are given as follows:

$$\sigma(\mathbf{J}_+) = \left\{ 2\cos\left(\frac{2k\pi}{N}\right), 1 \leq k < N/2 \right\} \cup \{-2, 2\}$$

$$\sigma(\mathbf{J}_-) = \left\{ 2\cos\left(\frac{2k-1\pi}{N}\right), 1 \leq k \leq N/2 \right\}.$$

Tables 2.1, 2.2, 2.3, and 2.4 below compare the eigenvalues computed from Algorithm 1 with the theoretical eigenvalues: the first six eigenvalues are displayed along with the error.* † Note that for these matrices of relatively large order, Algorithm 1 captures all but the last one or two digits of the theoretical eigenvalues. In the quadruple precision case for $\mathbf{J}_-$, the root-finding for the secular equation failed for two eigenvalues (not displayed in table). I believe this issue is minor, and perhaps some fine tuning in the deflation code is necessary.

---

*Fortran code and subroutines may be compiled to run in quadruple precision by promoting all `double precision` data types to `real*16`. This was accomplished in my implementation with the following script: `http://icl.cs.utk.edu/lapack-forum/viewtopic.php?f=2&t=2739`

†In my testing of these matrices from Gear, I used an sorting subroutine from the following website: `http://jean-pierre.moreau.pagesperso-orange.fr/`

Table 2.1 : First several eigenvalues of $\mathbf{J}_+$ computed with Algorithm 1 double precision. $N = 100000$.

exact	computed	error
-2.0000000000000000	-2.0000000000000004	0.0000000000000004
-1.9999999960521582	-1.9999999960521588	0.0000000000000007
-	-1.9999999960521586	0.0000000000000004
-1.9999999842086329	-1.9999999842086331	0.0000000000000002
-	-1.9999999842086331	0.0000000000000002
-1.9999999644694242	-1.9999999644694242	0.0000000000000000
-	-1.9999999644694242	0.0000000000000000
-1.9999999368345323	-1.9999999368345325	0.0000000000000002
-	-1.9999999368345323	0.0000000000000000
-1.9999999013039569	-1.9999999013039578	0.0000000000000009
-	-1.9999999013039573	0.0000000000000004

Table 2.2 : First several eigenvalues of $\mathbf{J}_-$ computed with Algorithm 1 double precision. $N = 100000$.

exact	computed	error
-1.9999999990130395	-1.9999999990130397	0.0000000000000002
-	-1.9999999990130395	0.0000000000000000
-1.9999999911173560	-1.9999999911173560	0.0000000000000000
-	-1.9999999911173556	0.0000000000000004
-1.9999999753259889	-1.9999999753259894	0.0000000000000004
-	-1.9999999753259892	0.0000000000000002
-1.9999999516389386	-1.9999999516389391	0.0000000000000004
-	-1.9999999516389384	0.0000000000000002
-1.9999999200562049	-1.9999999200562055	0.0000000000000007
-	-1.9999999200562051	0.0000000000000002
-1.9999998805777879	-1.9999998805777885	0.0000000000000007
-	-1.9999998805777881	0.0000000000000002

Table 2.3 : First several eigenvalues of $\mathbf{J}_+$ computed with Algorithm 1 in quadruple precision. $N = 100000$.

exact	computed	error
$-2.00000000000000000000000000000000$	$-2.00000000000000000000000000000000$	$0.00E+00$
$-1.99999999605215824086304443274865 58$	$-1.99999999605215824086304443274865 60$	$0.20E-33$
-	$-1.99999999605215824086304443274865 56$	$0.20E-33$
$-1.99999998420863297903763228618019 51$	$-1.99999998420863297903763228618019 53$	$0.20E-33$
-	$-1.99999998420863297903763228618019 49$	$0.20E-33$
$-1.99999996446942426128012716432242 53$	$-1.99999996446942426128012716432242 54$	$0.20E-33$
-	$-1.99999996446942426128012716432242 53$	$0.00E+00$
$-1.99999993683453216551780153545866 42$	$-1.99999993683453216551780153545866 53$	$0.12E-32$
-	$-1.99999993683453216551780153545866 44$	$0.20E-33$
$-1.99999901303956800848836424483200 7$	$-1.99999901303956800848836424483201 2$	$0.60E-33$
-	$-1.99999901303956800848836424483200 9$	$0.20E-33$

Table 2.4 : First several eigenvalues of $\mathbf{J}_-$ computed with Algorithm 1 in quadruple precision. $N = 100000$.

exact	computed	error
$-1.99999999013039559972238380642216$	$-1.99999999013039559972238380642216$	$0.40E-33$
-	$-1.99999999013039559972238380642215$	$0.20E-33$
$-1.99999991117356045594690885897309$	$-1.99999991117356045594690885897310$	$0.80E-33$
-	$-1.99999991117356045594690885897309$	$0.20E-33$
$-1.99999975325989048010504991396413$	$-1.99999975325989048010504991396414$	$0.60E-33$
-	$-1.99999975325989048010504991396414$	$0.40E-33$
$-1.99999951638938629561498764059546$	$-1.99999951638938629561498764059546$	$0.80E-33$
-	$-1.99999951638938629561498764059545$	$0.40E-33$
$-1.99999920056204883760398996622188$	$-1.99999920056204883760398996622188$	$0.40E-33$
-	$-1.99999920056204883760398996622188$	$0.00E+00$
$-1.99999880577787935290840838461846$	$-1.99999880577787935290840838461846$	$0.20E-33$
-	$-1.99999880577787935290840838461846$	$0.00E+00$

2.3.2 Fibonacci model

Most of the calculations in this thesis fall in the less-studied intermediate coupling regime. This range of λ values allows for implementation of Algorithm 1 in double precision since band widths shrink more slowly for smaller values of λ (see Figures 1.3 and 1.4). Calculations may be taken to a higher levels than calculated in this work as long as λ is sufficiently small to avoid exponentially close eigenvalues. In turn, quadruple precision calculations may be used to tackle larger values of the coupling strength (greater than 4) to resolve differences in close-by eigenvalues. It is possible to compile LAPACK routines to run in quadruple precision, but computational time increases due to quadruple precision arithmetic.

I have included tables of the 5 middle computed eigenvalues of the matrices $\mathbf{J}_{\pm}$ for the Fibonacci Hamiltonian. Values in the middle of the spectrum are chosen given the qualitative assumption that substantial clustering occurs in this region. Four different methods are shown: Algorithm 1 in double and quadruple precision, MATLAB's `eig`, and the LAPACK routine `DSYEV.f` compiled to run in quadruple precision.

Note the proximity of eigenvalues for this application since they approximate the Cantor spectrum of the Fibonacci Hamiltonian. One obtains more digits of accuracy for $\lambda = 2$ as compared to $\lambda = 8$ since the eigenvalue spacing decays more gradually in level k for smaller values of λ. The digits highlighted in grey are those of the eigenvalues computed in double precision in agreement with the digits of the eigenvalues computed in quadruple precision.

Table 2.5 : Five middle eigenvalues in $\sigma(\mathbf{J}_+)$ for the Fibonacci Hamiltonian with $\lambda = 2$. The order of $\mathbf{J}_+$ is 10946. Displayed are the computed eigenvalues from four separate codes, two in double precision and two in quadruple precision.

Alg. 1	1.429235757432078 4
`eig`	1.429235757432 107
Alg. 1	1.42923575743207823307203914571315 54
`DSYEV.f`	1.42923575743207823307203914571315 29
Alg. 1	1.42925333089613 50
`eig`	1.4292533308961 62
Alg. 1	1.42925333089613495210114494503187 25
`DSYEV.f`	1.42925333089613495210114494503187 34
Alg. 1	1.429288026199825 8
`eig`	1.4292880261998 44
Alg. 1	1.42928802619982565215165293491507 77
`DSYEV.f`	1.42928802619982565215165293491507 96
Alg. 1	1.42930620097212 20
`eig`	1.4293062009721 42
Alg. 1	1.42930620097212176776162613434703 80
`DSYEV.f`	1.42930620097212176776162613434704 03
Alg. 1	1.429340897878959 0
`eig`	1.4293408978789 83
Alg. 1	1.42934089787895934737175810903064 48
`DSYEV.f`	1.42934089787895934737175810903064 67

Table 2.6 : Five middle eigenvalues in $\sigma(\mathbf{J}_+)$ for the Fibonacci Hamiltonian with $\lambda = 8$. The order of $\mathbf{J}_+$ is 10946.

Alg. 1	7.1233218906775 511
`eig`	7.12332189067 9813
Alg. 1	7.123321890677507725905202799044127 8
`DSYEV.f`	7.123321890677507725905202799044137 1
Alg. 1	7.123321890896 7313
`eig`	7.12332189089 8212
Alg. 1	7.123321890896688529729648529547074 3
`DSYEV.f`	7.123321890896688529729648529547085 1
Alg. 1	7.123321893816 1196
`eig`	7.123321893816 916
Alg. 1	7.123321893816085286191027682314388 2
`DSYEV.f`	7.123321893816085286191027682314415 1
Alg. 1	7.1233218939197 620
`eig`	7.1233218939 20583
Alg. 1	7.123321893919727277658699006219234
`DSYEV.f`	7.123321893919727277658699006219527
Alg. 1	7.1233218968391 663
`eig`	7.1233218968 40594
Alg. 1	7.123321896839124054723065952432697 7
`DSYEV.f`	7.123321896839124054723065952432710 8

Table 2.7 : Five middle eigenvalues in $\sigma(\mathbf{J}_-)$ for the Fibonacci Hamiltonian with $\lambda = 2$. The order of $\mathbf{J}_-$ is 10946.

Alg. 1	1.4292404547761508
`eig`	1.4292404547761 90
Alg. 1	1.42924045477615084342295582441545 17
`DSYEV.f`	1.42924045477615084342295582441545 30
Alg. 1	1.429249324211662 8
`eig`	1.4292493242116 83
Alg. 1	1.42924932421166295188858970871850 01
`DSYEV.f`	1.42924932421166295188858970871850 07
Alg. 1	1.4292934828231283
`eig`	1.4292934828231 48
Alg. 1	1.42929348282312832921653715934091 64
`DSYEV.f`	1.42929348282312832921653715934091 64
Alg. 1	1.429300744352445 5
`eig`	1.4293007443524 59
Alg. 1	1.42930074435244561792241763210160 20
`DSYEV.f`	1.42930074435244561792241763210160 49
Alg. 1	1.429344904720694 1
`eig`	1.42934490472 0721
Alg. 1	1.42934490472069442193688226287727 15
`DSYEV.f`	1.42934490472069442193688226287727 15

Table 2.8 : Five middle eigenvalues in $\sigma(\mathbf{J}_-)$ for the Fibonacci Hamiltonian with $\lambda = 8$. The order of $\mathbf{J}_-$ is 10946.

Alg. 1	7.12332189068856 54
`eig`	7.1233218906 90949
Alg. 1	7.123321890688559331444500263677453 5
`DSYEV.f`	7.123321890688559331444500263677394 2
Alg. 1	7.1233218908903 284
`eig`	7.12332189089 1762
Alg. 1	7.123321890890308260100733739658964 6
`DSYEV.f`	7.123321890890308260100733739658979 2
Alg. 1	7.1233218938274 385
`eig`	7.12332189382 8312
Alg. 1	7.123321893827452044170021464176762 3
`DSYEV.f`	7.123321893827452044170021464176782 3
Alg. 1	7.1233218939083 329
`eig`	7.12332189390 9189
Alg. 1	7.123321893908360519786876855074300 2
`DSYEV.f`	7.123321893908360519786876855074320 2
Alg. 1	7.1233218968455 265
`eig`	7.12332189684 7012
Alg. 1	7.123321896845504324406252128739876 9
`DSYEV.f`	7.123321896845504324406252128739883 1

Chapter 3

Application: Fibonacci Hamiltonian

This chapter details an application of Algorithm 1 for computing the canonical covers $\sigma_k \cup \sigma_{k+1}$ of the spectrum Σ_λ of the Fibonacci Hamiltonian. Goals of these calculations include extrapolating approximations to fractal dimensions from the canonical covers and formulating combinatorial statements for the bands in σ_k in the coupling regime $\lambda \in (0, 4]$. Approximate dimensions inform conjectures regarding the regularity and mononoticity of the exact dimensions as functions of λ. Combinatorial results aide in extrapolation from the canonical covers, increase our physical understanding of quasicrystals, and unveil beautiful structure of theoretical interest. Relevant examples include the work of Killip et al., who present a complete description of the combinatorics for $\lambda > 4$ and then apply their result to derive bounds on quantum particle dynamics [16]. Similarly, Damanik, Embree, Gorodetski and Tcheremchantsev utilize these combinatorics to extrapolate bounds on fractal dimensions as λ tends to infinity; they then relate the box-counting dimension to the time evolution of an initial delta function [7]. My numerical work arises from the same motivations, but focuses on the less-studied intermediate coupling regime. Section 3.1 contains work on fractal dimensions and section 3.2 examines interval combinatorics.

3.1 Fractal dimensions

Two different dimensions, *box-counting* and *Hausdorff*, are defined as follows. Let $A \subset \mathbb{R}$.

Definition 3.1. *Let $\varepsilon > 0$ and $M_A(\varepsilon) = \#\{n \in \mathbb{Z} \ : [n\varepsilon, (n+1)\varepsilon) \cap A \neq \emptyset\}$. The upper and lower box-counting dimensions of A are respectively*

$$\dim_B^+ A = \limsup_{\varepsilon \to 0} \frac{\log M(\varepsilon)}{-\log \varepsilon}$$

$$\dim_B^- A = \liminf_{\varepsilon \to 0} \frac{\log M(\varepsilon)}{-\log \varepsilon}$$

*When the two limits above are equal, their limit, denoted $\dim_B A$, is the **box-counting** dimension of A.*

Definition 3.2. *Let $\Delta > 0$ and consider a set of intervals $\{C_l\}_{l \geq 1}$, such that $A \subset \bigcup_{l \geq 1} C_l$ and $|C_l| \leq \Delta$. Given the equation*

$$h^\alpha(A) = \lim_{\Delta \to 0} \inf_{\Delta\text{-}covers} \sum_{l \geq 1} |C_l|^\alpha$$

*with $\alpha \in [0, 1]$, the **Hausdorff** dimension is defined as*

$$\dim_H A = \inf\{\alpha : h^\alpha(A) < \infty\}.$$

The fractal dimensions of the spectrum Σ_λ reveal electronic transport properties of the Fibonacci Hamiltonian. For example, Theorem 3 in the paper of Damanik

et al. describes bounds the evolution of a portion of a wavepacket by a quantity involving a fractal dimension [7]. In addition, these dimensions give insight into the topological characteristics of spectra of two and three dimensional Fibonacci models. More precisely, higher dimensional models have spectra that are set sums of the one-dimensional spectrum Σ_λ. For two and three dimensions,

$$\sigma(\mathbf{H}_{2d,\lambda}) = \Sigma_\lambda + \Sigma_\lambda$$

$$\sigma(\mathbf{H}_{3d,\lambda}) = \Sigma_\lambda + \Sigma_\lambda + \Sigma_\lambda.$$

Since the one dimensional spectrum is a Cantor set, what can be said about the set sum of the set with itself? Damanik and Gorodetski relate the structure of the spectrum of the two-dimensional model with the box-counting dimension: $\sigma(\mathbf{H}_{2d,\lambda})$ is a Cantor set provided the upper box-counting dimension is less than $1/2$ [6]. Further, more subtle scenarios arise: the sum of a Cantor set with itself may form a *Cantorval*, an object with similarities to Cantor set and intervals. Definitions and related open problems may be found in the last section of the survey article [6].

Lastly, questions regarding regularity (and mononiticity) of the dimensions (with respect to λ) and the relationship between the two dimensions in the intermediate coupling regime remain open. In this section I discuss approximating dimensions of Σ_λ from the covers $\sigma_k \cup \sigma_{k+1}$ with a goal of shedding light on these open problems.

3.1.1 Approximating the Hausdorff dimension

I develop approximations to the Hausdorff dimension from the covers $\sigma_k \cup \sigma_{k+1}$ in a way derived from the work of Halsey et al.[13]. Papers from Kohmoto et al. and Tang et al. demonstrate an application of this approach to quasiperiodic models [17, 24], although they compute a different but related object, the "$f - \alpha$" curve of the spectrum.

To approximate the dimension, let $\{B_{j,k}\}_{j=1}^{N_k}$ be an enumeration of the bands in the cover $\sigma_k \cup \sigma_{k+1}$. With the bands $\sigma_k \cup \sigma_{k+1}$ and $\sigma_{k+1} \cup \sigma_{k+2}$, construct the following function:

$$g_k(\alpha) = \sum_{j=1}^{N_k} |B_{j,k}|^\alpha - \sum_{j=1}^{N_{k+1}} |B_{j,k+1}|^\alpha.$$

The approximate Hausdorff dimension is $\tilde{\alpha}_k$ such that $g_k(\tilde{\alpha}_k) = 0$. Qualitatively, one can view $\sigma_k \cup \sigma_{k+1}$ and $\sigma_{k+1} \cup \sigma_{k+2}$ as Δ-covers where k is taken large enough so Δ is sufficiently small. In turn, the assumption that both sums "suitably approximate" the limit $h^\alpha(\Sigma_\lambda)$ implies:

$$\frac{\sum_{j=1}^{N_k} |B_{j,k}|^\alpha}{\sum_{j=1}^{N_{k+1}} |B_{j,k+1}|^\alpha} \approx 1.$$

Enforcing equality of this ratio, I seek an approximate Hausdorff dimension as a root of g_k in $[0, 1]$. This root-finding procedure is done with MATLAB's `fzero` function. Table 3.1 depicts the approximate dimension calculated from successively higher levels; one observes convergence as k increases since the sets $\sigma_k \cup \sigma_{k+1}$ better approximates the Cantor spectrum.

Table 3.1 : Approximate Hausdorff dimension $\tilde{\alpha}$ computed with the covers $\sigma_k \cup \sigma_{k+1}$ and $\sigma_{k+1} \cup \sigma_{k+2}$.

k	λ =1	λ =2	λ =3	λ =4
3	0.629184721644038	0.546264141212987	0.550922327994936	0.488025115075937
4	0.771787611354064	0.638717166074610	0.496273486376101	0.436075223240581
5	0.768700800468207	0.598030704204576	0.524590522518344	0.464336767458792
6	0.785386181146746	0.617520701891302	0.509906155968885	0.448971753434186
7	0.770778331354799	0.608106601008542	0.517717324769096	0.457538829447008
8	0.780389915333086	0.612894523364685	0.513532576522766	0.452726564745786
9	0.776717523002441	0.610487449364452	0.515796329294084	0.455454717740420
10	0.771462300980417	0.611702134559407	0.514567334927181	0.453902527869412
11	0.773553577647827	0.611087938610503	0.515237426106680	0.454788987003961
12	0.772506384765335	0.611400513201802	0.514871488484564	0.454282020526147
13	0.772999910983101	0.611241269469838	0.515071697768937	0.454572409187434
14	0.772802368679696	0.611322506166104	0.514962086906362	0.454405989299610
15	0.772886942533129	0.611281039892397	0.515022143735560	0.454501424680883
16	0.772846521692368	0.611302226286371	0.514989228482746	0.454446685500930
17	0.772864775067337	0.611291396864031	0.515007274139668	0.454478089951739
18	0.772856924165551	0.611296934295102	0.514997379296334	0.454460072332500
19	0.772860487019160	0.611294102304395	0.515002805673527	0.454470411042160
20	0.772858831782941	0.611295550849554	0.514999829522381	0.454464482921194
21	0.772859571887832	0.611294809816774	0.515001463458351	0.454467874686662
22	0.772859243100286	0.611295188819406	0.515000573873506	0.454465912748311
23	0.772859393255526	0.611294994922469	0.515001056835674	0.454467035392032
24	0.772859 324719459	0.61129 5094167910	0.51500 0778375714	0.45446 5398123737

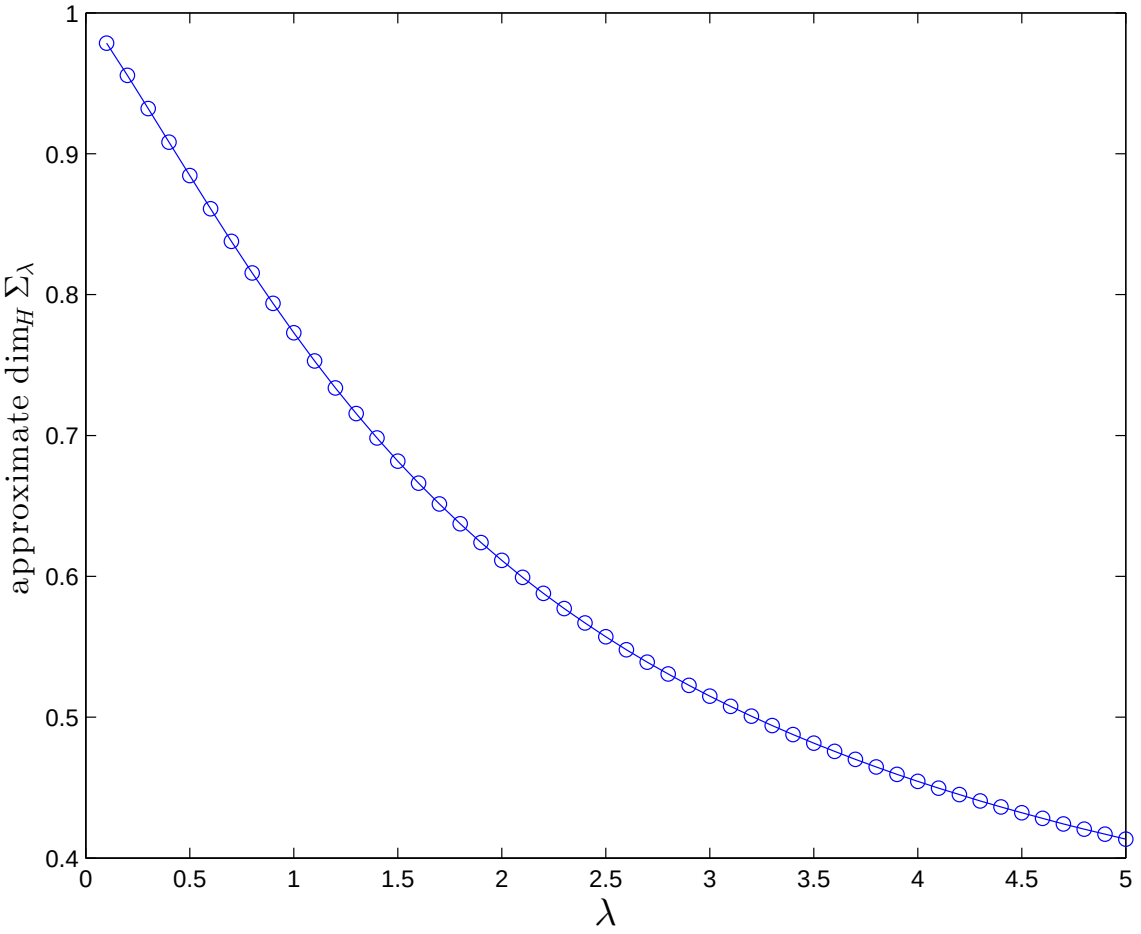

Figure 3.1 : Approximate Hausdorff dimension calculated from the covers $\sigma_k \cup \sigma_{k+1}$ with $k = 23, 24$.

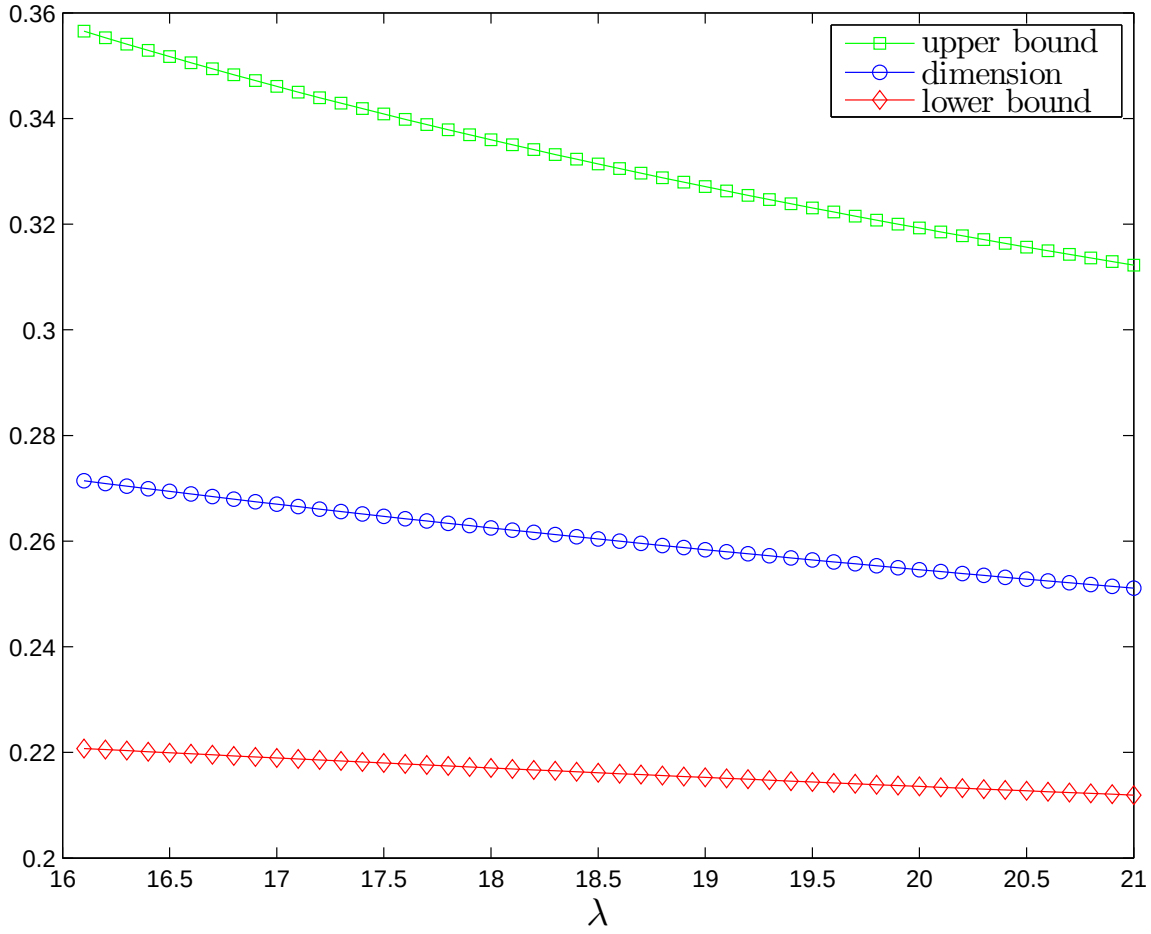

Figure 3.2 : Approximate Hausdorff dimension calculated from the covers $\sigma_k \cup \sigma_{k+1}$ with $k = 13, 14$. Also plotted are the upper and lower bounds proven in [7].

Figure 3.1 shows the approximate Hausdorff dimension as a function of λ. At this level of resolution in λ, the dimension appears to be monotone and contains no jumps; these observations support conjectures regarding regularity and monotonicity (i.e. Corollary 5.6 of [6] for a statement about regularity).

Damanik et al. derived upper and lower bounds on the the Hausdorff dimension for $\lambda > 16$ [7]. In their notation, with $S_u(\lambda) = \frac{1}{2}\left(\lambda - 4 + \sqrt{(\lambda-4)^2 - 12}\right)$ and $S_l(\lambda) = 2\lambda + 22$, they proved

$$\dim_H \Sigma_\lambda \geq \frac{\log(1+\sqrt{2})}{\log S_u(\lambda)}$$

and

$$\dim_H \Sigma_\lambda \leq \frac{\log(1+\sqrt{2})}{\log S_l(\lambda)}.$$

As a check of this method of approximation, I have plotted the approximated dimension and the bounds in Figure 3.2.

3.1.2 Box-counting dimension

Several conjectures regarding the box-counting dimension of Σ_λ require some numerical insight. For $\lambda > 16$ and sufficiently small, the box-counting and Hausdorff dimensions are equal, but less is known in the intermediate coupling regime (see [6]). Generally, the fractal dimensions of a set $A \subset \mathbb{R}$ satisfy

$$\dim_H A \leq \dim_B^- A \leq \dim_B^+ .$$

For the spectrum Σ_λ, Damanik et al. conjecture the equality of the dimensions for any $\lambda > 0$ [6].

In addition, numerical work may reveal critical λ values at which transitions in the spectrum of higher dimensional models occur, i.e. λ for which the upper box-counting dimension is equal to $1/2$. Assuming equality of the dimensions for all λ, Figure 3.1 suggests the dimension takes the value $1/2$ for $\lambda \approx 3$. Table 3.2 more precisely investigates this critical value of λ in the following way. I created a function taking $\lambda \mapsto$ (approximation of $\dim_H \Sigma_\lambda$) by efficiently computing the covers $\sigma_k \cup \sigma_{k+1}$ and $\sigma_{k+1} \cup \sigma_{k+2}$ with Algorithm 1, and then from these covers, extracting an approximation to the Hausdorff dimension as described in section 3.1.1. The values displayed in Table 3.2 are the roots of this function in the interval $[3, 4]$.

The relevant data collected from the covers $\sigma_k \cup \sigma_{k+1}$ for approximating the box-counting dimension are particular sequences of infima for each λ. More precisely, define the function

$$f_{k,\lambda}(\varepsilon) = \frac{\log M_{\sigma_k \cup \sigma_{k+1}}(\varepsilon)}{-\log \varepsilon}.$$

From Figures 3.3 and 3.4, one is hopeful that the sequence $\inf_{\varepsilon \in (0,1)} f_{k,\lambda}(\varepsilon)$ converges to the box-counting dimension of Σ_λ. These figures appear in the survey paper by Damanik, Embree, and Gorodetski, but without averaging over ε-grids. I compute the value of the function $f_{k,\lambda}$ at ε with averaging by shifting the ε-grid by $(j-1)\varepsilon/N$, where N is the number of realizations. For each $j = 1 \ldots N$, I compute a number $\frac{\log M_j}{-\log \varepsilon}$, where M_j is the number of intervals in the shifted grid that nontrivially intersect

Table 3.2 : Approximation of λ such that $\dim \Sigma_\lambda = 1/2$. This critical coupling strength is determined by approximating the Hausdorff dimension as discussed in section 3.1.1, and then determining a root of $\dim_H \Sigma_\lambda - 1/2$ in the interval $[3, 4]$.

k	root of $\dim_H \Sigma_\lambda - 1/2$
5	3.358132165787465
6	3.136023908556593
7	3.252443323604985
8	3.188369245375197
9	3.223061231166874
10	3.203897752346325
11	3.214420790092100
12	3.208597301692052
13	3.211813603439293
14	3.210032038473626
15	3.211018258537230
16	3.210471722049607
17	3.210774542902178
18	3.210606689833002
19	3.210699725856641
20	3.210648145088315
21	3.210676725662388
22	3.210661023369781

$\sigma_k \cup \sigma_{k+1}$; $f_{k,\lambda}(\varepsilon)$ is taken as the average over these values.

The approximate Hausdorff dimension as computed in Section 3.1.1 is plotted as a dashed line in Figures 3.3 and 3.4 with the plots of $f_{k,\lambda}$ to visualize the connection between the Hausdorff and box-counting dimensions. In all cases the dashed line provides a lower bound on the infima. Table 3.3 displays the sequence of minima for four values of the coupling strength: the convergence is agonizingly slow. From Figure 3.4 one expects quicker convergence for the largest value $\lambda = 4$, but even in this case I think we cannot expect even one digit of accuracy (for example, the first digit should be 4 if we assume equality of Hausdorff and box-counting). I have attempted Richardson extrapolation and other techniques, with no luck as of yet. My hope is that future work will lead to a robust extrapolation approach or other method for approximating the box-counting dimension from the covers $\sigma_k \cup \sigma_{k+1}$, and in turn clearly reveal the relationship between this dimension and the Hausdorff dimension. The combinatorics of the intervals in the canonical covers, discussed in the next section, will aide in this endeavor and expose some theoretically interesting structure.

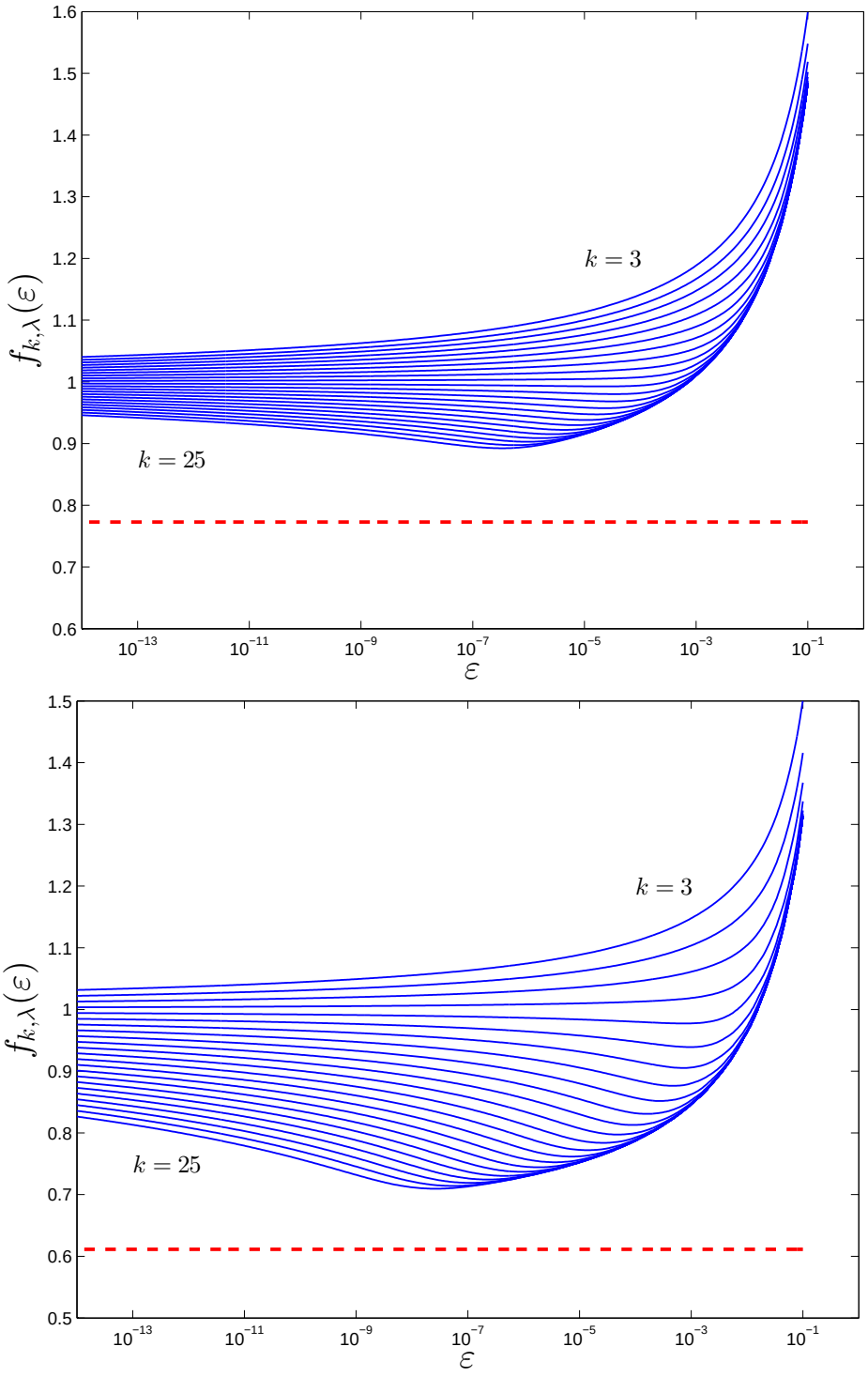

Figure 3.3 : Plot of $f_{k,\lambda}(\varepsilon)$ for $\lambda = 1$ (top) and $\lambda = 2$ (bottom). The dashed line indicates the approximate Hausdorff dimension computed with the covers $\sigma_k \cup \sigma_{k+1}$, $k = 24, 25$.

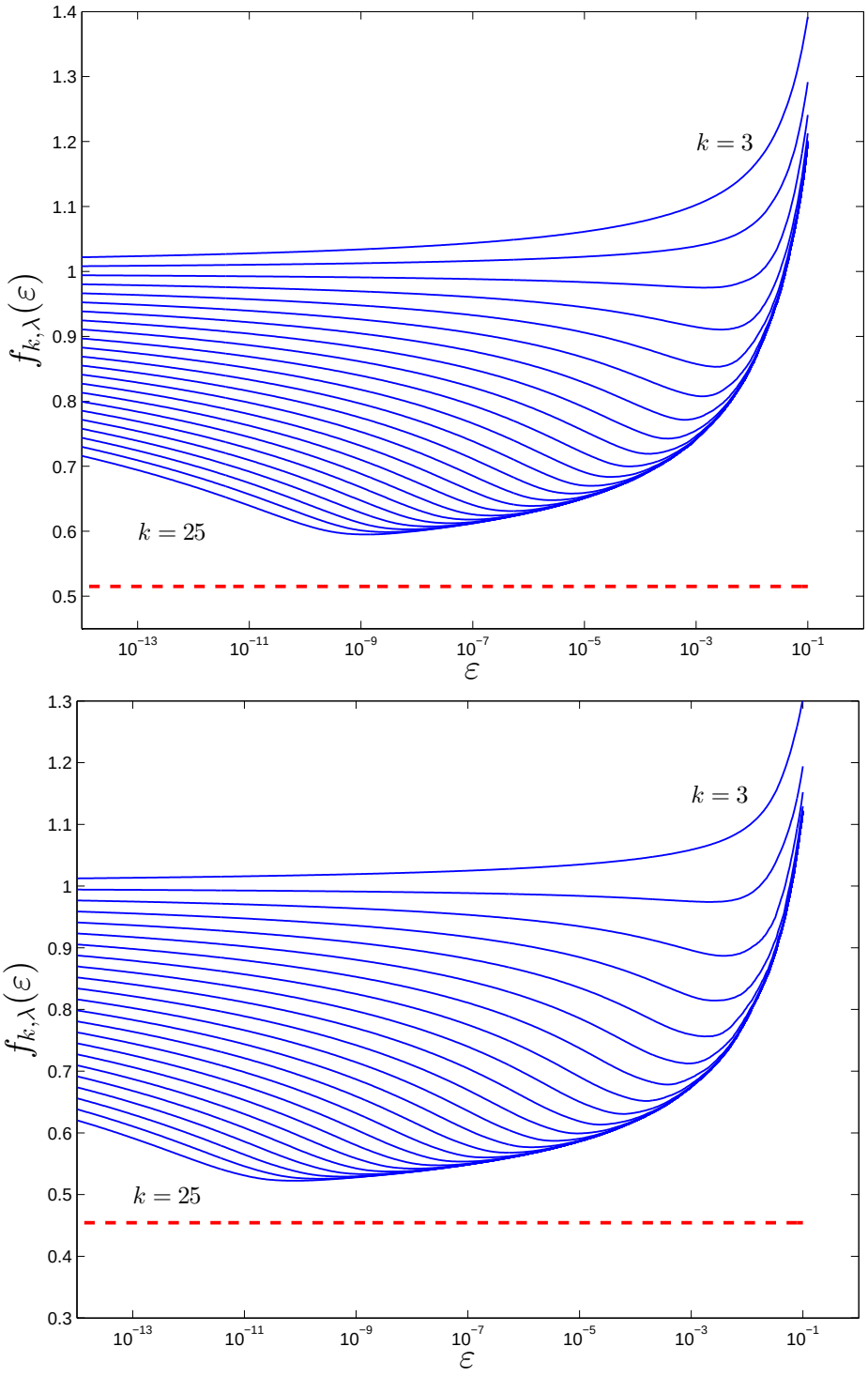

Figure 3.4 : Plot of $f_{k,\lambda}(\varepsilon)$ for $\lambda = 3$ (top) and $\lambda = 4$ (bottom). The dashed line indicates the approximate Hausdorff dimension computed with the covers $\sigma_k \cup \sigma_{k+1}$, $k = 24, 25$.

Table 3.3 : Minima of $f_{k,\lambda}$.

k	λ =1	λ =2	λ =3	λ =4
3	1.033690374357641	1.020910493677296	1.007675551433517	0.974304418307971
4	1.029832371980677	1.012171101846078	0.975057863829920	0.886970066967079
5	1.025760663005993	1.003343598705628	0.910501290843763	0.814212661765846
6	1.021788545212406	0.977335659216472	0.853068663203542	0.756153716774866
7	1.017710702651374	0.938994041090419	0.807642826684725	0.712396859144580
8	1.013662016174192	0.905192759373435	0.771390418305331	0.678195050411085
9	1.009608739156427	0.876265716691289	0.742439945370494	0.651646358103175
10	1.005558170184183	0.851659013898191	0.719155138002150	0.630658616541623
11	1.001505367486138	0.830783541758325	0.699701411751737	0.613257312436646
12	0.992630169065828	0.812790983485494	0.683608447321058	0.599090745660449
13	0.980191527069022	0.797255792166007	0.669854277701721	0.587111985902891
14	0.968326459019880	0.783829656260194	0.658056615880547	0.576735916911632
15	0.957390706904360	0.772021960403334	0.647948090283464	0.567943350183914
16	0.947348126864978	0.761624258804871	0.638960066851253	0.560224653899987
17	0.938193435821631	0.752438429378058	0.631098631809072	0.553447659580781
18	0.929862198910716	0.744277720210695	0.624151259319281	0.547489999647133
19	0.922203649774688	0.736920270156837	0.617942335980872	0.542139764995826
20	0.915211705763475	0.730321376184499	0.612402267809297	0.537382153910118
21	0.908814478489363	0.724388643040782	0.607401103828021	0.533084900142523
22	0.902904727019487	0.718983142550873	0.602868369591248	0.529209305004420
23	0.897452926230463	0.714027922698487	0.598762954086135	0.525680636458503
24	0.892430776780336	0.709520219291430	0.595008622209617	0.522471112852720

3.2 Interval Combinatorics

A deep understanding of the combinatorial properties of the bands in σ_k will provide crucial insight into the spectrum Σ_λ. In particular, precise combinatorics will refine extrapolation techniques for fractal dimensions. For example, the work of Damanik et al. demonstrates an application of combinatorial properties for $\lambda > 4$ to approximate the box-counting dimension as $\lambda \to \infty$ [7]. I am seeking statements of the same flavor as Lemma 3.1 below (from [16]) in the intermediate coupling regime $\lambda \in (0, 4]$. The authors first define two types of bands in σ_k.

Definition 3.3. *If $I_k \subset \sigma_k$ is in σ_{k-1}, then I_k is a type A band. If $I_k \subset \sigma_k$ is in σ_{k-2}, then I_k is a type B band.*

Then they proved the following lemma.

Lemma 3.1. *Assume $\lambda > 4$. Every type A band in σ_k contains only one type B band in σ_{k+2} and no others. Every type B band in σ_k contains only one type A band in σ_{k+1} and two type B bands in σ_{k+2} lying on either side of the band in the previous level.*

This statement may be visualized in Figure 3.5. It follows immediately that the number of bands in $\sigma_k \cup \sigma_{k+1}$ is $2F_k$, provided $\lambda > 4$. The proof of Lemma 3.1 relies on the fact that for $\lambda > 4$,

$$\sigma_k \cap \sigma_{k+1} \cap \sigma_{k+2} = \emptyset \text{ for all } k,$$

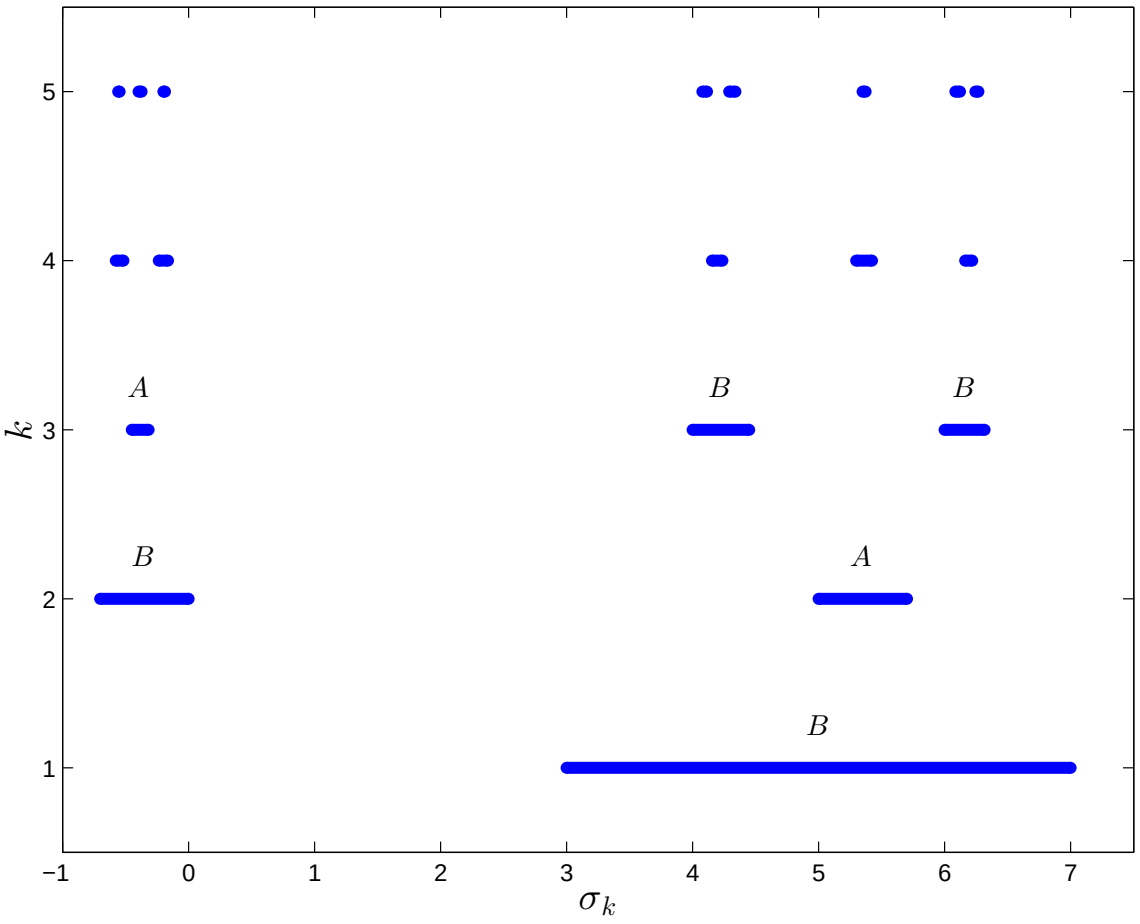

Figure 3.5 : Bands of σ_k for $k = 1, \ldots, 5$ with $\lambda = 5$.

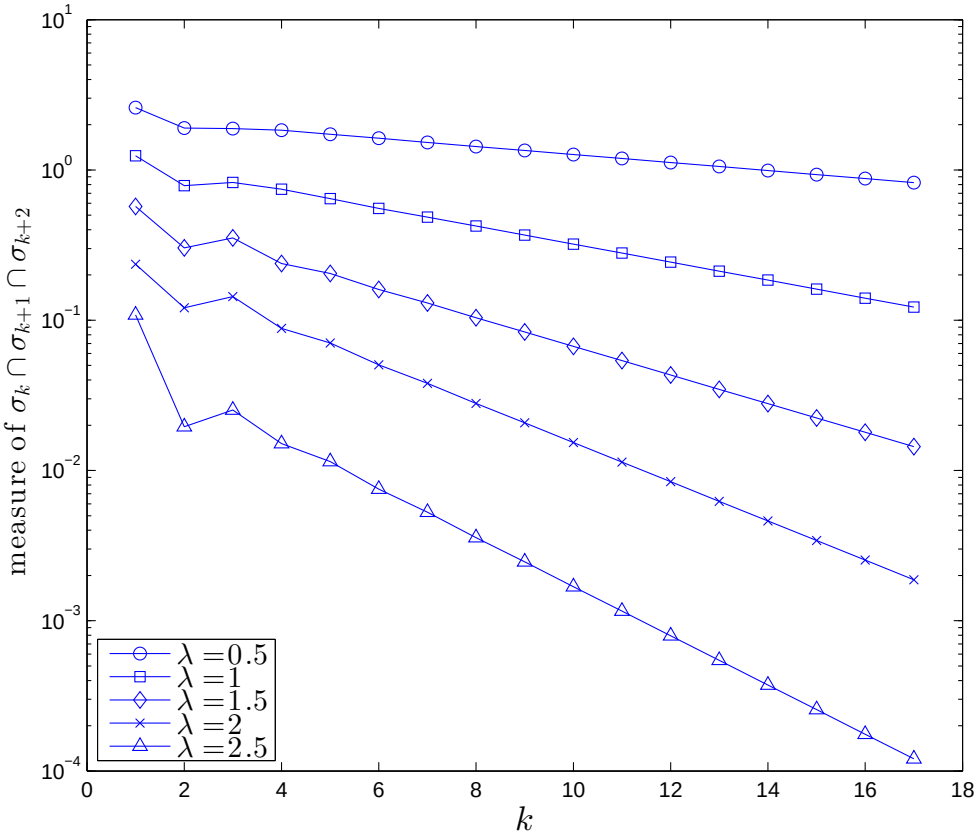

Figure 3.6 : Measure of the intersection $\sigma_k \cap \sigma_{k+1} \cap \sigma_{k+2}$.

which follows from the trace map and the equivalence $E \in \sigma_k \iff |x_k(E)| \leq 2$ (see Theorem 1.3).

I am interested in the intermediate values of the coupling strength greater than zero but less than 4; little is known regarding the combinatorial properties of the bands in σ_k (and the covers $\sigma_k \cup \sigma_{k+1}$) in this regime. Can similar statements be made for smaller values of λ? How do the bands in σ_k relate to bands in higher levels?

Figure 3.6 verifies a nontrivial intersection of three consecutive σ_k's for λ values

less than 4. Apparently the measure of the overlap eventually decays exponentially, with more rapid decay for larger λ values: the behavior of bands in three consecutive spectra approach the behavior proven for λ values greater than 4. How does this overlap behavior affect the combinatorics?

An investigation of the number of intervals in the covers $\sigma_k \cup \sigma_{k+1}$ reveals interesting structure. Table 3.4 exhibits the number of intervals in the canonical covers for various λ values less than 4. It appears that the sequence of the number of intervals *eventually* becomes Fibonacci regardless of the coupling strength, although further calculation is necessary for $\lambda < 0.75$. This observation resonates with the intuition that less overlap among consecutive σ_k's leads to accumulation of more bands in the covers.

Accurately counting the number of intervals in the numerically obtained set union $\sigma_k \cup \sigma_{k+1}$ presents a subtle challenge in light of floating point error and theoretically distinct eigenvalues that appear numerically "close." Hence for completeness, I have included Figure 3.7, which displays the minimum distance between end-points of intervals in σ_k and end-points of intervals in σ_{k+1}. The figure indicates several close eigenvalues for smaller k but nothing problematic for larger k that would disrupt the observed Fibonacci recurrence.

In light of the eventual Fibonacci recurrence ($N_k = N_{k-1} + N_{k-2}$, not necessarily with the convential Fibonacci starting values) depicted in Table 3.4, it is natural to investigate the point at which the recurrence appears in the sequence of number of

Table 3.4 : Number of intervals in $\sigma_k \cup \sigma_{k+1}$.

k	$\lambda = 0.25$	λ =0.5	λ =0.75	λ =1	λ =1.25	λ =1.5	λ =1.75	λ =2	λ =4.1
1	1	1	1	1	1	1	1	1	2
2	1	1	1	1	2	2	2	2	4
3	1	1	3	3	3	3	4	4	6
4	2	3	4	4	5	6	6	6	10
5	3	5	6	7	8	10	10	10	16
6	5	7	10	11	13	16	16	16	26
7	9	13	16	19	22	26	26	26	42
8	15	21	26	30	36	42	42	42	68
9	23	33	42	48	58	68	68	68	110
10	37	53	68	78	94	110	110	110	178
11	60	87	110	126	152	178	178	178	288
12	97	141	178	204	246	288	288	288	466
13	157	227	288	330	398	466	466	466	754
14	253	367	466	534	644	754	754	754	1220
15	411	595	754	864	1042	1220	1220	1220	1974
16	665	963	1220	1398	1686	1974	1974	1974	3194
17	1075	1557	1974	2262	2728	3194	3194	3194	5168
18	1739	2520	3194	3660	4414	5168	5168	5168	8362
19	2815	4078	5168	5922	7142	8362	8362	8362	13530
20	4555	6598	8362	9582	11556	13530	13530	13530	21892
21	7371	10676	13530	15504	18698	21892	21892	21892	35422
22	11925	17274	21892	25086	30254	35422	35422	35422	57314
23	19295	27950	35422	40590	48952	57314	57314	57314	92736
24	31221	45224	57314	65676	79206	92736	92736	92736	150050
25	50517	73174	92736	106266	128158	150050	150050	150050	242786

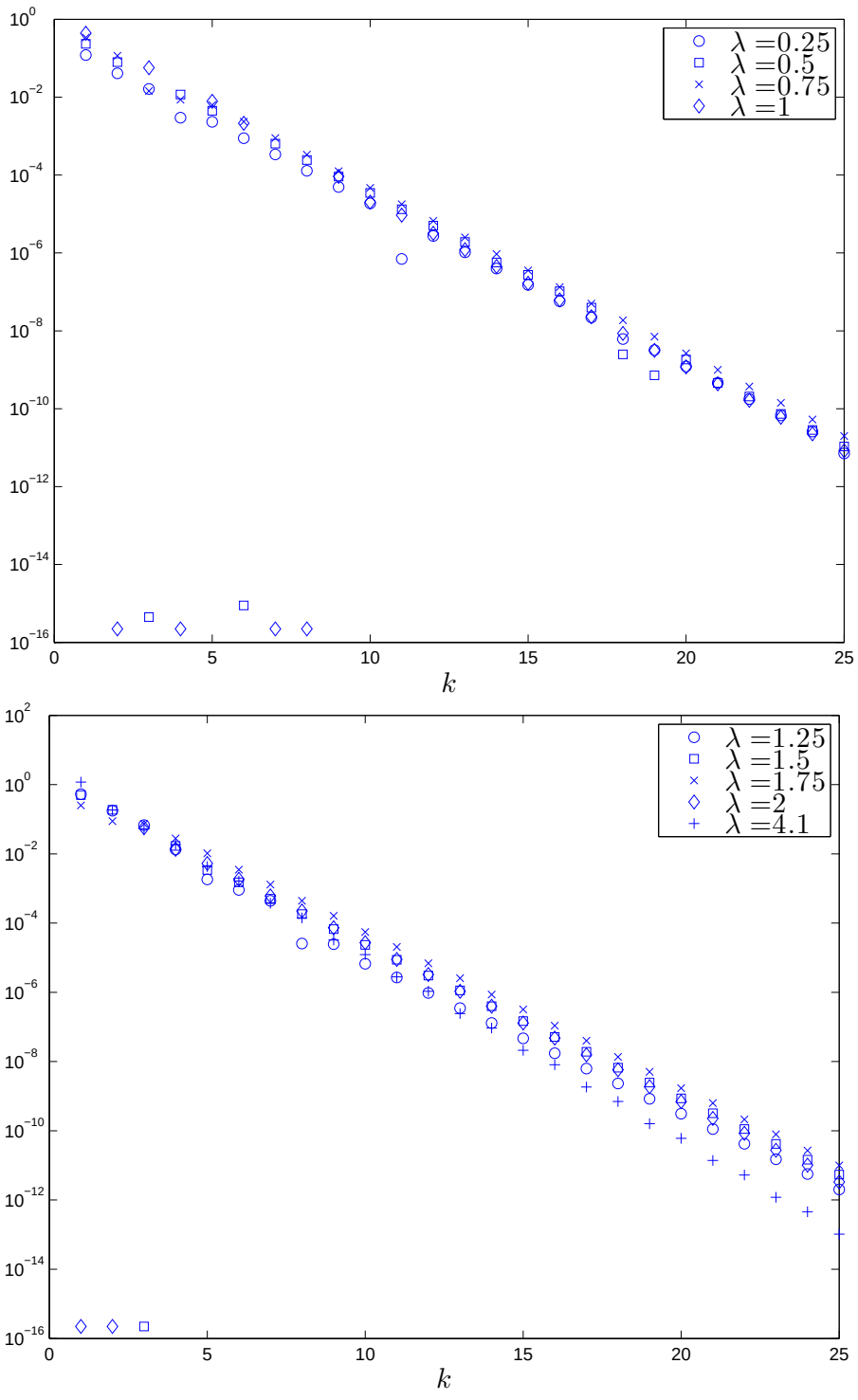

Figure 3.7 : Minimum distance between endpoints of the intervals in σ_k and endpoints of the intervals in σ_{k+1}.

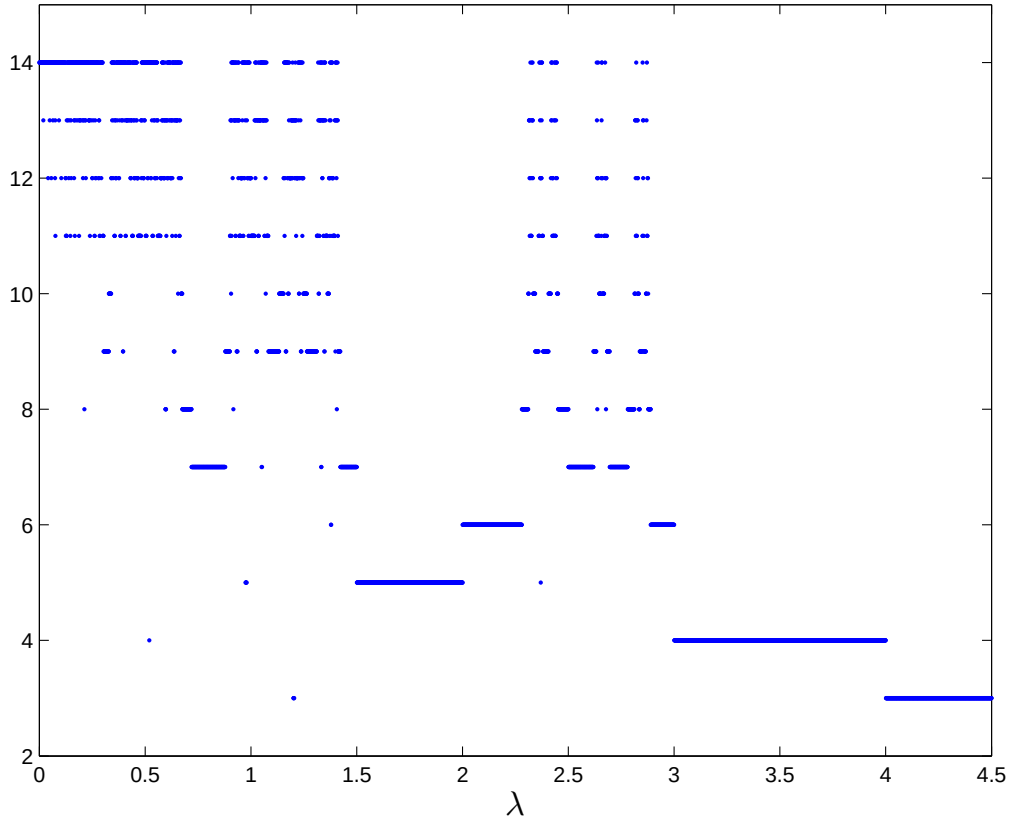

Figure 3.8 : Maximum level k (≥ 3) at which the number of intervals in $\sigma_k \cup \sigma_{k+1}$ does not obey the recurrence $N_k = N_{k-1} + N_{k-2}$.

intervals. This is done as follows: for a fixed λ, build a vector containing the number of intervals in $\sigma_k \cup \sigma_{k+1}$ for $k = 1, \ldots, 14$. Then, pick the maximum level (starting with $k = 3$) so that $N_k \neq N_{k-1} + N_{k-2}$. Figure 3.8 shows this maximum level for a fine mesh of λ values.

One can also investigate the number of intervals in the canonical covers as a function of λ. The figures given in the survey paper by Damanik, Embree, and Gorodetski elegantly display the canonical covers (k is fixed) as a functions of λ so that one clearly sees splitting of one interval into multiple intervals as λ increases [6].

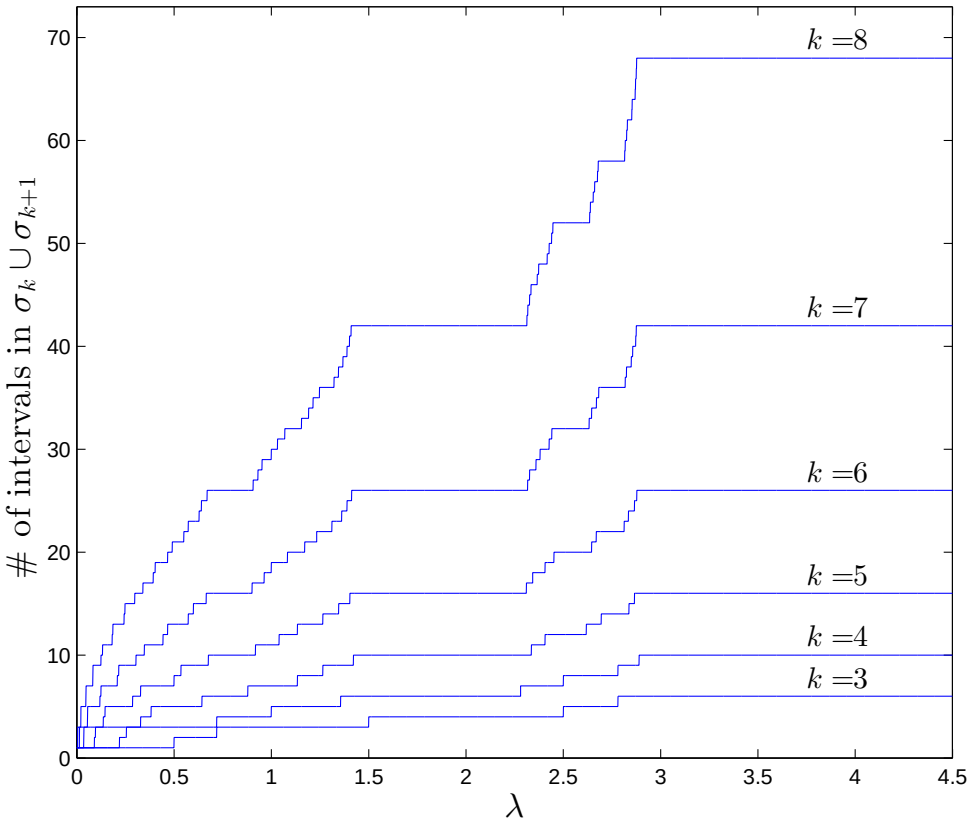

Figure 3.9 : Number of intervals in $\sigma_k \cup \sigma_{k+1}$ for several values of k.

Figure 3.9 demonstrates that this splitting occurs in a self-similar fashion. It appears the plateaus for a fixed k developing in between the more prominent plateaus form in systematic way, i.e. for $k = 8$, see the regions $1 < \lambda < 1.5$ and $2.5 < \lambda < 3$.

3.3 Concluding remarks and future work

This work presents an $O(n^2)$ algorithm for computing the spectra of periodic Jacobi operators and presents an application to a quasicrystal model, the Fibonacci Hamiltonian. More precisely, the sets σ_k, spectra of related periodic Jacobi operators, form

a cover $\sigma_k \cup \sigma_{k+1}$ for the Cantor spectrum of the Fibonacci Hamiltonian. Thus, by efficiently computing the sets σ_k with Algorithm 1, the Cantor spectrum may be approximated with the canonical covers. The sets $\sigma_k \cup \sigma_{k+1}$ allow one to numerically grasp the complicated Cantor structure of the spectrum with a goal of informing conjectures and gaining physical insight into quasicrystals.

The application Algorithm 1 to the Fibonacci model focused on the less-studied intermediate coupling regime $\lambda \in (0, 4]$. Future numerical work includes determining a more robust way of extrapolating the box-counting dimension from the canonical covers.

These numerical calculations motivate theoretical questions that require further investigation. What can be said about the regularity and monotonicity of the box-counting and Hausdorff dimensions in the intermediate coupling regime? Can one develop a closed-form expression for the fractal dimension from plots like Figure 3.1? Further, with perhaps more digits to the approximation in Table 3.2, can one conjecture and prove at what critical value of λ the dimension is equal to $1/2$? This endeavor naturally leads to further numerical and theoretical study of the two and three dimensional Fibonacci Hamiltonians.

Future work will also incorporate a theoretical investigation of the combinatorics of the intervals in the sets σ_k for λ in the intermediate coupling regime. I would like to rigorously explain the behavior observed in Figure 3.9 and Table 3.4. Can one prove that for any $\lambda > 0$, the number of intervals in the canonical covers eventually

obeys the Fibonacci recurrence? As a starting point, one can quickly show that for $\lambda > 2$,

$$\sigma_k \cap \sigma_{k+1} \cap \sigma_{k+2} \cap \sigma_{k+3} = \emptyset \text{ for all } k$$

by using the trace map. It would be interesting to use the above result and arguments adapted from Killip et al. to prove a statement similar to Lemma 3.1 [16]. I hope a better understanding of the combinatorics will help answer questions regarding fractal dimensions and in turn, contribute to our knowledge of quasicrystals.

Bibliography

[1] P. W. Anderson. Absence of Diffusion in Certain Random Lattices. *Phys. Rev.*, 109:1492–1505, 1958.

[2] P. Arbenz and G. Golub. On the Spectral Decomposition of Hermitian Matrices Modified by Low Rank Perturbations with Applications. *SIAM J. on Matrix Anal. Appl.*, 9(1):40–58, 1988.

[3] Peter Arbenz, Walter Gander, and Gene H. Golub. Restricted Rank Modification of the Symmetric Eigenvalue Problem: Theoretical Considerations. *Linear Algebra Appl.*, 104(0):75 – 95, 1988.

[4] J. R. Bunch, C. P. Nielsen, and D. C. Sorensen. Rank-One Modification to the Symmetric Eigenproblem. *Numer. Math.*, 31:31–38, 1978.

[5] P. Carpena, V. Gasparian, and M. Ortuño. Energy Spectra and Level Statistics of Fibonacci and Thue-Morse Chains. *Phys. Rev. B*, 51:12813–12816, May 1995.

[6] D. Damanik, M. Embree, and A. Gorodetski. Spectral Properties of Schrödinger Operators Arising in the Study of Quasicrystals. *Preprint*, 2012. date accessed: October 2012.

[7] D. Damanik, M. Embree, A. Gorodetski, and S. Tcheremchantsev. The Fractal Dimension of the Spectrum of the Fibonacci Hamiltonian. *Commun. Math. Phys.*, 280:499–516, 2008.

[8] James W. Demmel. *Applied Numerical Linear Algebra*. SIAM, Philadelphia, PA, 1997.

[9] N. Drake. Prospecting for Quasicrsytals. *Science News*, pages 24–26, November 2012.

[10] S. Even-Dar Mandel and R. Lifshitz. Electronic Energy Spectra and Wave Functions on the Square Fibonacci Tiling. *Philosophical Mag.*, 86(6-8):759–764, 2006.

[11] S. Even-Dar Mandel and R. Lifshitz. Electronic Energy Spectra of Square and Cubic Fibonacci Quasicrystals. *Philosophical Mag.*, 88(13-15):2261–2273, 2008.

[12] M. Gu and S. Eisenstat. A Stable and Efficient Algorithm for the Rank-One Modification of the Symmetric Eigenproblem. *SIAM J. Matrix Anal. Appl.*, 15(4):1266–1276, 1994.

[13] Thomas C. Halsey, Mogens H. Jensen, Leo P. Kadanoff, Itamar Procaccia, and Boris I. Shraiman. Fractal Measures and their Singularities: the Characterization of Strange Sets. *Phys. Rev. A*, 33:1141–1151, 1986.

[14] R. Ketzmerick, K. Kruse, S. Kraut, and T. Geisel. What Determines the Spreading of a Wave Packet? *Phys. Rev. Lett.*, 79:1959–1963, 1997.

[15] R. Ketzmerick, G. Petschel, and T. Geisel. Slow Decay of Temporal Corrrelations in Quantum Correlations with Cantor Spectra. *Phys. Rev. Lett.*, 69(5):695–698, 1992.

[16] Rowan Killip, Alexander Kiselev, and Yoram Last. Dynamical Upper Bounds on Wavepacket Spreading. *American J. of Math.*, 125(5):1165–1198, 2003.

[17] Mahito Kohmoto, Bill Sutherland, and Chao Tang. Critical Wave Functions and a Cantor-set Spectrum of a One-dimensional Quasicrystal Model. *Phys. Rev. B*, 35:1020–1033, 1987.

[18] Michael P. Lamoureux. Reflections on the Almost Mathieu Operator. *Integral Equations Operator Theory*, 28:45–59, 1997.

[19] Michihiro Naka, Kazusumi Ino, and Mahito Kohmoto. Critical Level Statistics of the Fibonacci Model. *Phys. Rev. B*, 71:245120, 2005.

[20] Gim Seng Ng and Tsampikos Kottos. Wavepacket Dynamics of the Nonlinear Harper Model. *Phys. Rev. B*, 75:205120, 2007.

[21] A. Sütő. The Spectrum of a Quasiperiodic Schrödinger Operator. *Commun. Math. Phys.*, 111:409–415, 1987.

[22] A. Sütő. Singular Continuous Spectrum on a Cantor Set of Zero Lebesgue Measure for the Fibonacci Hamiltonian. *J. Stat. Phys.*, 56:525–531, 1989.

[23] Yoshihiro Takada, Kazusumi Ino, and Masanori Yamanaka. Statistics of Spectra for Critical Quantum Chaos in One-dimensional Quasiperiodic Systems. *Phys. Rev. E*, 70:066203, 2004.

[24] Chao Tang and Mahito Kohmoto. Global Scaling Properties of the Spectrum for a Quasiperiodic Schrödinger Equation. *Phys. Rev. B*, 34:2041–2044, 1986.

[25] G. Teschl. *Jacobi Operators and Completely Integrable Nonlinear Lattices*. AMS, Providence, RI, 2000.

[26] D. J. Thouless. Bandwidths for a Quasiperiodic Tight-Binding Model. *Phys. Rev. B*, 28:4272–4276, 1983.

[27] Lloyd N. Trefethen and David Bau. *Numerical Linear Algebra*. SIAM: Society for Industrial and Applied Mathematics, Philadelphia, PA, June 1997.

[28] J. H. Wilkinson, editor. *The Algebraic Eigenvalue Problem*. Oxford University Press, Inc., New York, NY, USA, 1965.

[29] Michael Wilkinson and Elizabeth J. Austin. Spectral Dimension and Dynamics for Harper's Equation. *Phys. Rev. B*, 50:1420–1429, 1994.

[30] S. Willard. *General Topology*. Dover Books on Mathematics Series. Dover Publications, Incorporated, Mineola, NY, 1970.